Carbon dioxide degassing at the groundwater-stream-atmosphere interface: isotopic equilibration and hydrological mass balance in a sandy watershed

Loris Deirmendjian[1] and Gwenaël Abril[1, 2, *]

[1]Laboratoire Environnements et Paléoenvironnements Océaniques et Continentaux (EPOC), CNRS, Université de Bordeaux, Allée Geoffroy Saint-Hilaire, 33615 Pessac Cedex France.

[2]Departamento de Geoquímica, Universidade Federal Fluminense, Outeiro São João Batista s/n, 24020015, Niterói, RJ, Brazil.

*Now also at Laboratoire d'Océanographie et du Climat, Expérimentations et Approches Numériques (LOCEAN), Centre IRD France-Nord, 32, Avenue Henri Varagnat, F-93143 Bondy, France

Correspondence to Gwenaël Abril (g.abril@epoc.u-bordeaux1.fr)

Abstract

Streams and rivers emit significant amounts of CO_2 and constitute a preferential pathway of carbon from terrestrial ecosystems to the atmosphere. However, the estimation of CO_2 degassing based on water-air CO_2 gradient, gas transfer velocity and streams surface area, is subject to large uncertainties. Furthermore, the isotopic signature of DIC in streams is strongly impacted by gas exchange, which makes it a useful tracer of CO_2 degassing, under some specific conditions. For this study, we characterize annual transfers of dissolved inorganic carbon (DIC) along the groundwater-stream-river continuum based on DIC concentrations, isotopic composition and measurements of stream discharges. We selected as a study site a homogeneous, forested and sandy lowland watershed (Leyre River), where hydrology occurs almost exclusively through drainage of groundwater (no surface runoff). We observed a first general spatial pattern of pCO_2 and DIC decrease and δ^{13}C-DIC increase from groundwater to stream orders 1 and 2, which was due to a faster degassing of groundwater ^{12}C-DIC compared to ^{13}C-DIC, as verified experimentally. This downstream enrichment in ^{13}C-DIC could be modelled by simply considering the isotopic equilibration of groundwater-derived DIC with the atmosphere while CO_2 degassing. A second spatial pattern occurred between stream orders 2 and 4, consisting in an increase in the proportion of carbonate alkalinity to the DIC accompanied with enrichment in ^{13}C in stream DIC, was due to the occurrence of carbonates rocks weathering downstream. We could separate the contribution of these two processes (gas exchange and carbonates weathering) in the stable isotope budget of the river network. Thereafter, we build a hydrological mass-balance based on drainage factors and the relative contribution of groundwater in streams of increasing orders. After combining with dissolved CO_2 concentrations, we quantify CO_2 degassing in each stream orders for the whole watershed. About 75 % of the total CO_2 degassing from the watershed occurs in first and second order streams. Furthermore, from stream orders 2 to 4, our CO_2 degasing fluxes compared well with those based on stream hydraulic geometry, water pCO_2, gas transfer velocity, and stream surface area. In first order streams however, our approach gave CO_2 fluxes twice larger, suggesting a fraction of degassing occurred as hotspots at the vicinity of groundwater resurgence and was missed by conventional stream sampling.

Keywords: River systems, headwaters, carbon stable isotopes, CO_2 evasion, hotspot

1. Introduction

River networks have been recognized as an important component of the global carbon cycle. Indeed, world rivers transport yearly 0.9 Pg C from the continent to the ocean (Meybeck, 1982). This number based on a carbon concentration at various river mouths worldwide (Martin and Meybeck, 1979; Meybeck, 1981), corresponds to the global continental C input to estuarine and coastal systems (Borges, 2005). However, streams, lakes and rivers do not only act as a passive pipe that delivers terrestrial carbon to the ocean, but also as sites of CO_2 evasion to the atmosphere (Cole et al., 2007). Indeed, riverine waters are generally supersaturated in CO_2 compared to the overlying atmosphere, and this water-air gradient leads to CO_2 degassing (Frankignoulle et al., 1996; Cole et al. 2007). At the global scale, a recent estimate of CO_2 degassing in streams and rivers is 1.8 Pg C yr^{-1} (Raymond et al., 2013). This degassing flux is of the same order of magnitude as the net global CO_2 uptake by the terrestrial biosphere (Ciais et al., 2013) . In addition, the amount of carbon that originally leaves the terrestrial biosphere is much larger than the amount of terrestrial carbon that ultimately reaches the ocean (Cole et al., 2007).

The CO_2 dissolved in riverine waters originates from two different sources and processes (Hotchkiss et al., 2015): it can be (1) internal, i.e. resulting from heterotrophic decomposition and photo-oxidation of organic matter in the aquatic system itself or (2) external, i.e. resulting from inputs of groundwater enriched in CO_2, which comes from plant roots respiration and from microbial respiration of terrestrial organic matter in soils and groundwaters. However, sources of and processes controlling CO_2 emissions change with the size of streams and rivers (Hotchkiss et al., 2015). In headwaters (small streams), degassing is mainly of external origin and thus largely dependent on groundwater inputs and the catchment characteristics including lithology, topography, soil types, climate and vegetation (Lauerwald et al., 2013; Polsenaere et al., 2013). As stream orders and river discharge increase, soil and groundwater CO_2 inputs become less significant compared to internal CO_2 production. Hence, in larger rivers, internal processes become a more significant source of CO_2 degassing (Hotchkiss et al., 2015), but still based on terrestrial organic carbon losses (Cole and Caraco, 2001). Moreover, several studies on headwaters have been conducted in temperate (Butman and Raymond, 2011; Polsenaere and Abril 2012), boreal (Wallin et al., 2013; Kokic et al., 2015) and tropical (Johnson et

al., 2008; Davidson et al., 2010) ecosystems, at different spatial scales. These works converged to the same conclusion that headwaters are hotspots of CO_2 degassing, i.e., as regions that exhibit disproportionately high reaction rates relative to the surrounding area (Vidon et al., 2010). However, this hotspot character makes difficult a precise quantification of CO_2 evasion based on the water-air CO_2 gradient, the gas transfer velocity and the water surface area. Indeed, the two latter parameters are sometimes difficult to quantify accurately in headwaters (Raymond et al., 2012).

Dissolved Inorganic Carbon (DIC) in river systems includes not only dissolved CO_2 (CO_2*), but also carbonates and bicarbonates ions, generally quantified by alkalinity titrations assuming that Total Alkalinity (TA) is in majority carbonate alkalinity. TA originates from atmospheric CO_2 through the process of weathering of carbonates, silicates as well as other rocks (Meybeck, 1987; Amiotte-Suchet et al., 2003; Cai et al., 2008). Stable isotope composition of DIC (δ^{13}C-DIC) is both controlled by the signature of the carbon sources and the in-stream fractionating processes that change the δ^{13}C signature downstream (Brunet et al., 2005; Doctor et al., 2008; Polsenaere and Abril, 2012). On the one hand, oxidation of terrestrial organic matter liberates DIC with a quiet negative δ^{13}C signal, close to that of the dominating plants and soils in the watershed, i.e., between -22 and -34 ‰ for C_3 plants and -12 to -16 ‰ for C_4 plants (Vogel et al., 1993). In the other hand, weathering of carbonates rocks and minerals which have a δ^{13}C of about 0 ‰ (Clark and Fritz, 1997) makes δ^{13}C value of the DIC less negative. In addition, gas exchange along river courses increases the δ^{13}C signal of the DIC downstream because atmospheric CO_2 have δ^{13}C of about -7.5 ‰ (Keeling et al., 1984), making degassing of $^{12}CO_2$ faster than that of $^{13}CO_2$ (Polsenaere and Abril, 2012; Venkiteswaran et al., 2014). Thus, in aquatic systems with a limited amount of well identified carbon sources, and where fractionation factors can be calculated as the case for gas exchange, the origin and cycling of riverine DIC can be traced with δ^{13}C-DIC. In the case of headwaters, the isotopic signature of DIC is particularly useful, as it is governed by three major processes: input of ^{13}C depleted carbon from soils in majority as dissolved CO_2, eventually some inputs of ^{13}C enriched carbon from carbonates weathering in the form of alkalinity, and isotopic equilibration with the atmosphere induced by gas exchange (Polsenaere and Abril, 2012; Venkiteswaran et al., 2014).

In this study, we first focus on the link between CO_2 degassing and the isotopic signature of DIC along the groundwater-stream-river continuum. We selected as study site a small lowland temperate catchment, which offers the convenience of low slopes, a relatively homogeneous lithology (sands) and vegetation (pine forest), as well as a simple hydrological functioning mainly as groundwater drainage (no surface runoff). We couple isotopic models with experimental and *in situ* measurements to understand the dynamic of CO_2 degassing at two different scales (groundwater-stream interface and watershed). Our isotopic model quantitatively explains the relative importance of isotopic equilibration with the atmosphere and soil and carbonates rocks contributions to the DIC along the river continuum. We demonstrate that when drainage predominates, groundwaters and streams sampling can be coupled to discharge measurements to quantify CO_2 degassing, avoiding the necessity of assuming or measuring a gas transfer velocity and a water surface area, two parameters difficult to quantify and subject to a large variability at regional and global scales.

2. Material and Methods

2.1. Study site

The Leyre watershed is located in the southwestern part of France near Bordeaux and has a surface area of 2,100 km². The Leyre River flows 115 km northwest before reaching the Arcachon Lagoon (Fig. 1). The Leyre catchment is a very flat coastal plain with a mean slope lower than 1.25 ‰ and a mean altitude lower than 50 m (Jolivet et al., 2007). The lithology is relatively homogeneous and constituted of different sandy permeable surface layers dating from the Plio-quaternary period (Legigan, 1979) (Fig. 1). However, some sandy carbonated outcrops dating from the Miocene era are present locally (Fig. 1). The region was a vast wetland until the XIXth century, when a wide forest of maritime pine (*Pinus pinaster*) was sown following landscape drainage from 1,850. Nowadays, the catchment is mainly occupied by pine forest (about 84 %), with a modest proportion of croplands (about 14 %). The climate is oceanic with mean annual air temperature of 13°C and mean annual precipitation of 930 mm (Moreaux et al., 2011). Moreover, the average annual evapotranspiration is in the range of 234-570 and 63-800 mm, respectively for maritime pine and cropland (Govind et al., 2012). Owing to the low slope (i.e., < 1.25 ‰) and the high permeability (i.e., overall hydraulic conductivity is about 10^{-4} m s^{-1}, Corbier et al., 2010) of the soil, surface runoff cannot take place in the Leyre watershed, and thus the excess of rainfall percolates into the soil and supports the enrichment of carbon in groundwater. The soil permeability, the vegetation and the climate turn soils into podzols with an extremely coarse texture (Augusto et al., 2010). These podzols are characterized by a low pH (~4), low organic nutrient availability, and high organic carbon content that can reach 55 g per kg of soil (Jolivet et al., 2007). The sandy permeable surface layers contain a free and continuous groundwater table strongly interconnected with the superficial river network. This interconnection is facilitated by a dense network of drainage ditches, initiated in the XIXth century, and currently maintained by forest managers in order to increase tree growth rate. The seasonal changes in groundwater table can be important, with a water table close to the surface during wet winters and levelling down to 2.0 m depth below the surface during most summers. The groundwater table is also characterized by a period of discharge (i.e., when the groundwater level decreased) and a period of reload (i.e., when the groundwater level increased). In order to categorize the catchment

hydrology we use the Strahler classification but slightly modified. We define order 0 as groundwater and order 1 as streams and ditches either having no tributaries or being seasonally dry (from June to November during our sampling period). With these definitions, the stream orders in the Leyre watershed range from 0 (groundwater) to 4 (main river). In addition, hydrology is characterized by a period of highest flow in winter with a flood peak usually in February or March and a period of lowest flow in spring, summer and autumn.

2.2. Sampling strategy and field work

2.2.1. Selection and characterization of stations

We selected 21 sampling stations (18 river stations and 3 piezometers) within the watershed, from groundwater (order 0) to stream order 4 (main stem), after a precise characterization of the drainage basin based with a geographical information system (Fig. 1; Tab. 1). We included in the GIS the land use from the Corine Land Cover (2006) database, as well as the hydrological superficial network as a polyline form on an open water database (BD CARTHAGE ®). The BD CARTHAGE ® allows determine precisely the length of all streams in the watershed (Tab. 1). Based on digital elevation model (DEM) provided by French geographic institute (IGN), we divided the Leyre watershed in different sub-watersheds and we calculated their respective surface areas using ArcGIS 10.2^{TM} (Fig. 1; Tab. 1). The combination (with spatial analyst extension) of the DEM and the river network (transformed in a form point shapefile beforehand) allow assign an altitude for each river point and thus determinate the mean slope (S) per stream orders (Tab. 1).). We made one river width measure per campaign for each studied stations with either a decameter or a laser rangefinder (Tab. 1). We also sampled one groundwater spring and its respective headwater 40 meters downstream. The selected stations in stream orders 1 to 4 have all a sub-watershed occupied by at 80-100 % of forest (Tab. 1).

Concerning river discharge and depth, our study took benefit from four calibrated gauging stations of the French water quality agency (with a daily temporal resolution for river discharge, and with a one hour time resolution for depth), located on two second order streams (the Grand Arriou (GAR) and the Bourron (BR)), one third order stream (the Petite Leyre (PL)) and one fourth order stream (the Grande Leyre

(GL)) (Fig. 1; Tab. 1-2). For each stream order, we calculated the drainage factors and parameter α with a daily temporal resolution for a two years period (Tab. 2). The parameter α is the ratio (drainage ratio) between two drainage factors (i.e., discharge divided by the corresponding catchment area, in $m^3\ km^{-2}\ d^{-1}$) of streams of successive orders (Tab. 2). Because no gauging stations were available in first order streams, we complete our hydrological dataset by performing river flow measurements on two first order streams at high flow (Feb. 2016) and at base flow (Apr. 2015) (Tab. 2). In these first order streams, we measured water velocity profiles in river section with a magnetic induction current meter (OTT MF pro^{TM}), and we integrated the water velocity profiles in order to convert water velocity to discharge. As there is no surface runoff in the Leyre watershed the increase in drainage factors (hence the drainage ratio is > 1) between two streams of increasing orders allows a very precise quantification of additional diffusive groundwater inputs (Tab. 2).

In order to fully characterize the stream geometry in the Leyre watershed, we used the hydraulic equations described in Raymond et al. (2012). We estimate width (W), depth (D) and velocity (V), for each stream orders as follows (Tab. 1):

$W = aQ_{mean}^{\ b}$; $D = cQ_{mean}^{\ d}$; $V = eQ_{mean}^{\ f}$

Where,

a, c, e are geometry coefficients equal to 12.88, 0.4, 0.29, respectively, and b, d, f are geometry exponents equal to 0.42; 0.29; 0.29, respectively (Raymond et al. 2012). Q_{mean} is the mean river flow per stream orders (Tab. 1).

We used the mean width (estimated from Raymond et al., 2012) and the cumulated river length per stream order (estimated from BD CARTHAGE ®) to calculate the stream surface area per stream order (Tab. 1). We also used the parameters W, D, V and S to determine the gas transfer velocity in each stream orders, using the 7 empirical equations determined in Raymond et al (2012) (Tab. 1).

2.2.2. Field work

The 21 stations were visited with a frequency of approximately one month, on 18 occasions between Jan. 2014 and Jul. 2015. Exceptions were one piezometer that was visited on 16 occasions between Feb. 2014 and Jul. 2015 and two other

232 piezometers that were visited on 11 occasions between Aug. 2014 and Jul. 2015. In
233 addition, we also sampled on 5 occasions between Mar. 2015 and Jul. 2015, a
234 groundwater spring and its respective headwater 40 meters downstream. This
235 headwater has a mean depth of 5 cm and a mean width of 20 cm. We estimated the
236 discharge of this small headwater at two different periods (Feb. 2015 and Jul. 2015).
237 For that, we used a calibrated bucket and we timed how long it took to fill it. We
238 repeat this operation 10 times for the two different periods.

239 In total, we collected 292 samples for the concomitant measurements of temperature,
240 pH, pCO_2, TA, calculated DIC and δ^{13}C-DIC.

241 In the field, the partial pressure of CO_2 (pCO_2) in groundwater, stream and river
242 waters was measured directly using an equilibrator (Frankignoulle and Borges, 2001;
243 Polsenaere et al., 2013). This equilibrator was connected to an Infra-Red Gas
244 Analyzer (LI-COR®, LI-820), which was calibrated one day before sampling, on two
245 linear segments because of its non-linear response in the range of observed pCO_2
246 values (0–90,000 ppmv). This non-linearity was due to saturation of the IR cell at
247 pCO_2 values above 20,000 ppmv. We used certified standards (Air Liquide™ France)
248 of 2,079±42; 19,500±390 and 90,200±1,800 ppmv, as well as nitrogen flowing
249 through soda lime for the zero. For the first linear segment [0-20,000 ppmv], which
250 corresponded to river waters, we set the zero and we span the LI-COR at 19,500
251 ppmv, and we checked for linearity at 2,042 ppmv. For the second segment [20,000-
252 90,000 ppmv], which corresponded to the sampled groundwaters, we measured the
253 response of the LICOR with the standard at 90,000 ppmv, and used this measured
254 value to make a post correction of the measured value in the field. For groundwaters,
255 we took the precaution to renew the water in the piezometers by pumping of about
256 300 L with a submersible pump before sampling.

257 The δ^{13}C-DIC and DIC samples were collected using 120 mL glasses serum bottles
258 sealed with a rubber stopper and poisoned with 0.3 mL of $HgCl_2$ at 20 g L^{-1} to avoid
259 any microbial respiration during storage. Vials were carefully sealed taking care that
260 no air remained in contact with samples. Vials are also stored in the dark to prevent
261 photo-oxidation. We stored TA sampled in polypropylene bottles after filtration using
262 a syringe equipped with glass fiber (0.7 µm). We also measure pH (± 0.05) and
263 temperature (± 0.05 °C) *in situ* with specific probe (Metrhom). Before the start of each
264 sampling trip the pH probe was calibrated using NBS buffer solutions (4, 7 and 10).

2.3. Laboratory analysis

The $\delta^{13}C$-DIC was measured following the procedure of Gillikin and Bouillon (2007). A headspace was first created in the 120 mL serum vial, by injecting 25 mL of Helium gas. Then 0.3 mL of warm 85% phosphoric acid was added in order to titrate all bicarbonates and carbonates to CO_2. To ensure gas equilibration the vials were strongly shaken. Measurements were performed using Isotope Ratio Mass Spectrometer (Micromass Isoprime), equipped with a manual gas injection port. We injected twice 2 mL of headspace gas from the vial headspace. The carbon isotope ratio is expressed in the delta notation ($\delta^{13}C$) relative to Pee Dee Belemnite. $\delta^{13}C$-DIC was calibrated against a homemade standard (45 mg of Na_2CO_3 were introduced in a sealed vial flushed with helium, and were then dissolved with 3 mL of warm 85 % phosphoric acid); this standard had been calibrated against a certified standard (NBS19, -1.96 %) using a dual-inlet IRMS (Micromass Isoprime). The isotopic value of the Na_2CO_3 standard was -4.5±0.2 ‰. Finally, to correct for the partitioning of CO_2 between headspace and the water phase in the samples, and to calculate the $\delta^{13}C$ of the total DIC, the isotopic fractionation of CO_2 at the water-air interface as a function of lab temperature of Miyajima et al (1995) was applied.

TA was analyzed on filtered samples by automated electro-titration on 50 mL filtered samples with 0.1N HCl as titrant. Equivalence point was determined with a Gran method from pH between 4 and 3 (Gran, 1952). Precision based on replicate analyses was better than ± 5 µM. For samples with a very low pH (<4.5), we bubbled the water with atmospheric air in order to degas CO_2. Consequently, the initial pH increased above the value of 5, and TA titration could be performed (Abril et al., 2015).

We calculated DIC from pCO_2, TA, and temperature measurements using carbonic acid dissociation constants of Millero (1979) and the CO_2 solubility from Weiss (1974) as implemented in the CO_2SYS program. We also performed some direct measurements of DIC on a selection of 239 samples. DIC was measured in an extra sealed 120 mL serum vial, after creating a headspace of 25 mL with nitrogen gas, acidifying with 0.3 mL of 85% phosphoric acid, and shaking. Gas mixture from the headspace was analysed by injecting through a septum 0.5 mL of gas in a closed loop connected to the LICOR LI-820 (air flow 0.5 L min^{-1}). Soda lime was placed after

298 the gas analyser and ensures a zero baseline at the entrance of the IRGA. Peak
299 areas were recorded, integrated and compared to those obtained with standards
300 made by dissolving well-known amounts of $CaCO_3$ in distilled water at the
301 atmospheric pCO_2. pH and TA were also measured to check the calculated DIC
302 concentration in these standards. DIC concentrations in the samples were calculated
303 from the water and headspace volumes and the solubility coefficient of CO_2 from
304 (Weiss, 1974). DIC measured directly was consistent with DIC calculated from pCO_2
305 and TA at ±15% for a DIC range of 90-5,370 µmol L^{-1}. Therefore, we report here the
306 DIC dataset based on calculation with pCO_2 and TA.

307

308 **2.4. Degassing experiment**

309 We performed experimental degassing of dissolved CO_2 in order to understand how
310 δ^{13}C-DIC is affected when CO_2 originating from the groundwater degasses to the
311 atmosphere. We collected two 10 L containers of groundwater on the field, filled until
312 the top without air to limit degassing. The water was poisoned immediately in the field
313 with $HgCl_2$ to inhibit respiration. Back in the laboratory, we pumped this water to the
314 equilibrator to monitor continuously the pCO_2. The outlet of the equilibrator was
315 connected to the container, recirculating the water in a closed circuit. When the value
316 of pCO_2 was stable we collected a 120 mL vial to perform δ^{13}C-DIC measurements
317 thereafter. Then, we aerated the water by bubbling air from the outside (thus
318 containing CO_2 close to the atmospheric concentration and isotopic value, i.e., 400
319 ppmv and -7.5 ‰) using an air pump and a bubbling system. When the decrease of
320 pCO_2 was sufficient (for increments between 8,000 and 100 ppmv depending on the
321 concentration), we stopped the aeration, wait for a stable pCO_2 signal, and sample
322 again for δ^{13}C-DIC measurements. We repeated this operation until the water pCO_2
323 was equilibrated with the atmosphere. We also measured TA, before and after each
324 experiment. The experiment was reproduced on two occasions, and we obtained a
325 total of 35 pairs of pCO_2 and δ^{13}C-DIC values, or pairs of calculated DIC and δ^{13}C-
326 DIC values, after verifying that TA was not affected by degassing and constant during
327 the experiment.

328

3. Calculations

3.1. Modelling DIC isotopic equilibration during CO_2 degassing

We modelled changes in δ^{13}C-DIC during CO_2 degassing on the basis of equations detailed in the StreamCO_2-DEGAS, first created by Polsenaere and Abril (2012).

3.1.1. Initial state of $\delta^{13}C\text{-}CO_2^*$ in river

The model operates between pH 4.7 and 7.2 because between these values DIC can be simply considered as the sum of CO_2^* from oxidation of terrestrial organic matter and HCO_3^- from rock weathering. Model takes into account mass conservation of the DIC, using the apparent CO_2 solubility constant K_0 (mmol L^{-1} atm^{-1}) of Weiss (1974) for freshwater. In the calculation, TA is assumed as conservative and not affected by gas exchange.

$$\delta^{13}C\text{-}DIC \cdot [DIC] = \delta^{13}C\text{-}CO_2^* \cdot [CO_2^*] + \delta^{13}C\text{-}HCO_3^- \cdot [TA] \quad \text{(Eq. 1)}$$

In river water dissolved CO_2 (CO_2^*) is in isotopic equilibrium with bicarbonates as defined by Zhang et al (1995).

$$\delta^{13}C\text{-}HCO_3 = \delta^{13}C\text{-}CO_2^* + \varepsilon \quad \text{(Eq. 2)}$$

With,

ε represents the isotopic fractionation (‰) of HCO_3^- relatively to dissolved CO_2^*.

Thus, the initial stable isotopic composition of dissolved CO_2 is obtained from (Eq. 1) and (Eq. 2):

$$\delta^{13}C\text{-}CO_2^*{}_{initial} = \delta^{13}C\text{-}DIC_{initial} + ((\varepsilon * [TA]_{initial}) / [DIC]_{initial}) \quad \text{(Eq. 3)}$$

Where,

$\delta^{13}C\text{-}CO_2^*{}_{initial}$ and $\delta^{13}C\text{-}DIC_{initial}$ are the stable isotopic composition of initial dissolved CO_2 and initial DIC, respectively.

3.1.2. Partial pressure of $^{12}CO_2$ and $^{13}CO_2$ in air and water

The initial partial pressures of $^{12}CO_2$ and $^{13}CO_2$ in river waters can be calculated from the water pCO_2 starting from (Eq. 4).

$$p^{13}CO_{2water\ initial} = \delta^{13}C\text{-}PDB \cdot pCO_{2initial} \cdot ((\delta^{13}C\text{-}CO_{2initial}^* / 1000) + 1) / 1 + \delta^{13}C\text{-}PDB \cdot ((\delta^{13}C\text{-}CO_{2initial}^* / 1000) + 1) \quad \text{(Eq. 4)}$$

Where,

$p^{13}CO_{2water\ initial}$ is the initial partial pressure of $^{13}CO_2$ in water (ppmv) and δ^{13}C-PDB refers to Pee-Dee belemnite standard isotope equal to 0.011237.

Then, C stable isotopes in CO_2 follow the mass conservation in water as in (Eq. 5), and the Henry's law as in (Eq. 6).

$$[CO_2^*]_{water} = [^{12}CO_2^*]_{water} + [^{13}CO_2^*]_{water} \quad \text{(Eq. 5)}$$

$$pCO_{2\ water} \,.\, K_0 = p^{12}CO_{2\ water}\, K_0 + p^{13}CO_{2\ water} \,.\, K_0 \quad \text{(Eq. 6)}$$

Similarly for the atmosphere, the partial pressures of each CO_2 stable isotope in the air can be calculated using (Eq. 7) and (Eq. 8).

$$p^{13}CO_{2atmosphere} = \delta^{13}\text{C-PDB} \,.\, pCO_{2atm} \,.\, ((\delta^{13}\text{C-}CO_{2atmosphere} / 1000) + 1) / 1 + \delta^{13}\text{C-PDB} \,.\, ((\delta^{13}\text{C-}CO_{2atmosphere} / 1000) +1) \quad \text{(Eq. 7)}$$

Where,

$p^{13}CO_{2atmosphere\ initial}$ is the initial partial pressure of $^{13}CO_2$ in the atmosphere (ppm) and $\delta^{13}\text{C-}CO_{2atmosphere}$ equates to -7.5 ‰.

Then, CO_2 stable isotopes follow the mass conservation in the air:

$$pCO_{2\ atmosphere} = p^{12}CO_{2\ atmosphere} + p^{13}CO_{2\ atmosphere} \quad \text{(Eq. 8)}$$

3.3.3. Water-air gradient and flux of $^{12}CO_2$ and $^{13}CO_2$

The model calculates CO_2 fluxes to the atmosphere for each isotope from the following equations:

$$F^{13}CO_2 = k_{600}K_0 (p^{13}CO_{2water} - p^{13}CO_{2atmosphere}) \quad \text{(Eq. 9)}$$

Where,

$F^{13}CO_2$ represents the $^{13}CO_2$ fluxes at the interface in mmol m^{-2} h^{-1}; K_0 is the apparent CO_2 solubility constant of Weiss (1974) in mol kg^{-1} atm^{-1}; k_{600} is an arbitrary normalized gas transfer velocity (for a Schmidt number of 600 in cm h^{-1}).

Afterwards, the model calculates a loss of CO_2 ($[CO_2^*]_{loss}$) from river to the atmosphere for each isotope from the different water-air gradient.

$$[^{13}CO_2^*]_{loss} = (k_{600}t/10^{-3}H)K_0\Delta p^{13}CO_2 = \beta K_0(p^{13}CO_{2water} - p^{13}CO_{2atmosphere}) \quad \text{(Eq. 10)}$$

Where,

$[^{13}CO_2^*]_{loss}$ is the loss of $^{13}CO_2$ to the atmosphere in mmol L-1, t is a time constant (h) and H is the depth of the river (m); both t and H are arbitrarily fixed as their values do

not affect the model results (Polsenaere and Abril 2012). The same calculations are made for $^{12}CO_2$ fluxes and dissolved $^{12}CO_2$ losses. In Equation (10), the term β is dimensionless and proportional to the ratio between the gas transfer velocity and water height. As the same value of β is applied to both isotopes, this parameter can be fixed arbitrarily and defines the size of the iterations. In the model, the relationship between CO_2 degassing and δ^{13}C-DIC is not affected by β, by the chosen gas transfer velocity or by the river depth (Polsenaere and Abril 2012).

3.3.4. Loss of DIC and change in δ^{13}C-DIC

The $[CO_2^*]_{loss}$ is removed from the concentration of $^{12}CO_2^*$ and $^{13}CO_2^*$.

$$[^{13}CO_2^*]_{n+1} = [^{13}CO_2^*]_n - [^{13}CO_2^*]_{loss} \quad \text{(Eq. 11)}$$

$$[^{12}CO_2^*]_{n+1} = [^{12}CO_2^*]_n - [^{12}CO_2^*]_{loss} \quad \text{(Eq. 12)}$$

$$[CO_2^*]_{n+1} = [^{13}CO_2^*]_{n+1} + [^{12}CO_2^*]_{n+1} \quad \text{(Eq. 13)}$$

$$[DIC]_{n+1} = [CO_2^*]_{n+1} + [TA] \quad \text{(Eq. 14)}$$

When the new concentration of DIC is obtained the model calculates the new δ^{13}C as in (Eq. 15)

$$\delta^{13}\text{C-DIC}_{n+1} = (\delta^{13}\text{C-}CO_2^*{}_{n+1} \,.\, [CO_2^*]_{n+1} + [TA] \,.\, \delta^{13}\text{C-}HCO_3^-{}_{n+1}) \,/\, ([CO_2^*]_{n+1} + TA) \quad \text{(Eq. 15)}$$

Where,

$$\delta^{13}\text{C-}CO_2^*{}_{n+1} = (([^{13}CO_2^*]_{n+1} \,/\, [^{12}CO_2^*]_{n+1}) \,/\, \delta^{13}\text{C-PDB}) - 1) \,.\, 1000 \quad \text{(Eq. 16)}$$

$$\delta^{13}\text{C-}HCO_3^-{}_{n+1} = \delta^{13}\text{C-}CO_2^*{}_{n+1} + \varepsilon \quad \text{(Eq. 17)}$$

Finally, from the new δ^{13}C of the total DIC the new concentration of the DIC is calculated.

4. Results

4.1. Hydrology and water mass balance in the Leyre Watershed

During the monitoring period (Jan. 2014-Jul. 2015), hydrology was characterized by an average discharge of 21.3 $m^3 s^{-1}$ at the most downstream station (Fig. 1; 2a), including two relatively short flood events (further referred as “high flow period”) in Jan. 2014 – Apr. 2014 (maximum flow 120 $m^3 s^{-1}$) and in Feb. 2015 – Mar. 2015 (maximum flow 60 $m^3 s^{-1}$), and two longer periods of low flow (further referred as “base flow period”) between May. 2014 – Jan. 2015 and Apr. 2015 – Jul. 2015 (minimum flow 5.1 $m^3 s^{-1}$ in Nov. 2014). Periods for groundwater discharging (decreasing water table) were Jan. 2014 – Oct. 2014 and Mar. 2015 - Jul. 2015, and period of groundwater loading (increasing water table) was Nov. 2014 – Mar. 2015 (Fig. 2a).

The spatial increase in drainage ratios (i.e., parameter α) between streams of successive orders provides an estimate of additional water flows from diffusive groundwater inputs in higher stream order reaches, compared to that coming from the streams immediately upstream (because there is no surface runoff in the Leyre watershed) (Tab. 2).. This assumption is further checked when we closed the mass balance of DIC with the calculated water budget (see part 4.3). We found the following drainage ratios (i.e., parameter α) between discharges in streams of increasing orders (Tab. 2):

$$Q_{Or2}=1.83\pm0.53Q_{Or1} \quad \text{(Eq. 18)}$$

$$Q_{Or3}=1.20\pm0.36Q_{Or2} \quad \text{(Eq. 19)}$$

$$Q_{Or4}=1.05\pm0.15Q_{Or3} \quad \text{(Eq. 20)}$$

These downstream increases in drainage reflect the contributions of groundwater drainage (GW) in each stream order, relative to runoff from upstream. Thus, the water balance in the Leyre Watershed during the two years periods (Jan. 2014-Dec. 2015) can be described as follows:

$$Q_{Or2}=Q_{Or1}\ (55\%) + GW_{1\text{-}2}\ (45\%) \quad \text{(Eq. 21)}$$

$$Q_{Or3}=Q_{Or2}\ (83\%) + GW_{2\text{-}3}\ (17\%) \quad \text{(Eq. 22)}$$

$$Q_{Or4}=Q_{Or3}\ (95\%) + GW_{3\text{-}4}\ (5\%) \quad \text{(Eq. 23)}$$

Thus,

$Q_{Or4} = \Sigma Q_{Or2}$ (79%) + GW_{2-3} (16%) + GW_{3-4} (5%) (Eq. 24)

$Q_{Or4} = \Sigma Q_{Or1}$ (43%) + GW_{1-2} (36%) + GW_{2-3} (16%) + GW_{3-4} (5%) (Eq. 25)

Where,

Q_{Or1}, Q_{Or2}, Q_{Or3} and Q_{Or4} refer to river flow of each stream order and GW_{1-2}, GW_{2-3} and GW_{3-4} refer to groundwater inputs in each stream order.

River depths (D), widths (W), and velocities (V) modelled with hydraulic equations of Raymond et al (2012) for each stream order in the Leyre watershed are shown in Table 1, together with the available measurements of these three parameters. The modelled values of D compared very well (less than 15% difference) with those observed daily at the gauging stations in streams with order 2, 3 and 4. In the Leyre basin, the river network for stream orders 1 and 2 is highly human-managed. Hence, the modelled width values compared well with those measured in the field (Tab. 1). In contrast, in the Leyre basin, third and fourth order streams are natural and thus the spatial variability of width is higher than in streams order 1 and 2. Hence, in streams the modelled with values are further away from those measured in the field (Tab. 1). The modelled river velocities increased from less than 10 cm per second in first order streams to a maximum of 50 cm per second in fourth order streams. V values in first order streams were consistent with those measured in a headwater and a relatively large first order stream (Tab.1).

4.2. Spatio-temporal variations of pCO_2, TA, DIC and δ^{13}C-DIC

Throughout the sampling period, pCO_2, TA, DIC and isotopes ratios of DIC varied greatly in time (Fig. 2) and space (Tab. 3; Fig. 3) along an upstream-downstream gradient (from groundwaters to fourth order stream). A significant decrease of pCO_2 was observed while river order was increasing (Fig. 3a). Mean pCO_2 values were 48,070±26,320; 4,820±4,540; 3,000±1,090; 1,740±580 and 1,740±460 ppmv for groundwaters, first, second, third and fourth order streams, respectively (Tab. 3; Fig. 3). Temporally, the stronger variations of pCO_2 occurred in groundwaters and first order streams (Fig. 2b). In groundwaters, an increase of pCO_2 (from 7,700 to 103,870±12,510 ppmv) occurred during discharging periods (Fig. 2a-b). In contrast, a rapid decrease of pCO_2 (down to 28,890±2,790 ppmv in Mar. 2015) was observed during loading periods, when groundwater was apparently diluted with rainwater (Fig.

2a-b). The same temporal trend occurred in first order streams, although with an amplitude much smaller (3,700±1,530-27,205 ppmv) than in groundwaters (7,680-103,870±12,510 ppmv) (Fig. 2b). Moreover, in first order streams highest value of pCO_2 (27,205 ppmv in Sep. 2014) was associated with lowest value of groundwater table during base flow period (Fig 2a-b). In second, third and fourth order streams, water pCO_2 followed a seasonal cycle asymmetric compared to groundwaters, with lower pCO_2 values during base flow and higher pCO_2 values during flood peaks (Fig. 2a-b).

During the entire sampling period, TA values were not significantly different ($p>0.05$) in groundwaters, first and second order streams (Tab. 3; Fig. 3b). Indeed, mean values of TA were 71±25, 74±45 and 90±60 µmol L^{-1} respectively for groundwaters, first and second order streams (Tab. 3; Fig. 3). In contrast, a significant increase ($p<0.001$) of TA was observed between second and third order streams and between third and fourth order streams ($p<0.05$), where mean values of TA were 230±190 and 300±110 µmol L^{-1} respectively for third and fourth order streams (Tab. 3; Fig. 3b). Throughout the sampling period, the results did not show important temporal variations of TA in groundwaters, in first order streams and in second order streams (Tab. 3; Fig. 2c). Temporal variations were observed only in third order streams (range 65±15 - 410±280 µmol L^{-1}) and fourth order stream (range 100±40 - 480±25 µmol L^{-1}) (Fig. 2). Seasonally, TA in third and fourth order streams increased during groundwater discharging period and decreased during groundwater loading period, to reach a minimum value during flood peak (Fig. 2a-c).

DIC concentrations and isotopic composition showed a clear spatial trend along the groundwater-stream-river continuum (Fig. 3c-d). Indeed, DIC concentrations significantly decreased ($p<0.001$) from 2,300±1,120 µmol L^{-1} in groundwaters to 310±210 µmol L^{-1} in first order streams (Tab. 3; Fig. 3c). In parallel, δ^{13}C-DIC increased from -26.2±1.2 ‰ in groundwaters to -19.8±2.7‰ in first order streams (Tab. 3; Fig. 3d). More downstream, DIC concentrations remained globally constant ($p>0.05$) in first (mean is 310±210µmol L^{-1}), second (240±65µmol L^{-1}) and third (310±180µmol L^{-1}) order streams, and finally significantly increase ($p<0.05$) in fourth order streams (380±100µmol L^{-1}) (Tab. 3; Fig. 3). The latter increase was related to an increase of TA (Fig. 3b), and was also concomitant with a significant ($p<0.01$) increase of δ^{13}C-DIC from -16.2±4.4 ‰ in third order streams to -14.1±2.4‰ in fourth

506 order stream (Tab. 3; Fig. 3d). Temporal variations of DIC followed those of pCO_2 in
507 groundwaters (range from 570 to 4,590±2,700 µmol L^{-1}) and in first order streams
508 (range from 225±25 to 1280 µmol L^{-1}) (Fig. 2b-d). On the contrary, temporal
509 variations of DIC in third order streams (range from 145±15 to 490±270 µmol L^{-1}) and
510 fourth order stream (range from 215±80 to 550±30 µmol L^{-1}) followed those of TA
511 (Fig. 3c-d). Stable isotopes compositions of DIC were globally constant in
512 groundwaters (-26.2±1.2 ‰) (Tab. 3; Fig. 2). Furthermore, during base flow periods
513 (May. 2014 – Jan. 2015 and Apr. 2015 – Jul. 2015), δ^{13}C-DIC signal was also overall
514 stable in first order streams (-18.9±2.4 ‰), second order streams (-18.5±2.2 ‰), third
515 order streams (-14.9±2.5 ‰), and fourth order stream (-12.9±0.7 ‰) (Fig. 2e). In
516 contrast, during the flood peaks (Feb. 2014 and Mar. 2015) we observed a significant
517 decrease of δ^{13}C-DIC in headwaters (down to -27.6 ‰ in Mar. 2015 in first order
518 streams) and rivers (down to -28.9, -35.4 and -21.1 ‰ in Mar. 2015 for second, third
519 and fourth order streams respectively). This was particularly true during the second
520 flood event (Fig. 2e).

521

522 **4.3. Spring waters**

523 We sampled a groundwater spring and its very small headwater 40 meters
524 immediately downstream. This sampling was made in order to see how fast CO_2
525 degassing could occur in very small streams and also how δ^{13}C-DIC signal could be
526 affected when CO_2 that originates from groundwater is degassed to the atmosphere.
527 All the discharge in the stream was apparently coming from the sampled spring. For
528 the five sampling periods, values of pCO_2 in the spring were 22,370; 30,000; 32,170;
529 34,950 and 37,500 ppmv whereas those in the headwater (40 meters downstream)
530 were 6,560; 9,950; 10,100; 11,050 and 10,900 ppmv. On average, spring waters had
531 lost 70% of their dissolved CO_2 in 40 meters. Values of δ^{13}C-DIC were -26.7; -26.7; -
532 24.7; -24.6 and -25.6 ‰ in the spring whereas they were -20.4;-21.5;-21.9; -21.6 and
533 -19.5 ‰, in the headwater. Consequently, for the five sampling periods, pCO_2 has
534 lost 21,700±6,800 ppmv in 40 meters; in the meantime δ^{13}C-DIC increased by
535 +4.7±1.7 ‰. In addition, for a mean water velocity of 5 cm s^{-1}, the travel between the
536 spring and the sampling point in the headwater (40 meters downstream) was covered
537 in about 10 minutes. Thereafter, we tried to reproduce experimentally these field
538 observations in order to compare it with our isotopic model.

539

540 **4.4. Degassing experiment**

541 The two degassing experiments allowed describing well how δ^{13}C-DIC is affected
542 when CO_2 originating from the groundwater degasses to the atmosphere (Fig. 4).
543 Initial pCO_2 values were 41,160 and 47,730 ppmv, TA concentrations were 35 and 70
544 µmol L^{-1}, DIC concentrations were 1,720 and 2,030 µmol L^{-1}, and δ^{13}C-DIC values
545 were -26.2±0.1 ‰ and -26.5±0.04 ‰ for the two experiments, respectively. Final
546 pCO_2 values were 530 and 460 ppmv, TA concentrations were 35 and 70 µmol L^{-1},
547 DIC concentrations were 55 and 90 µmol L^{-1}, and δ^{13}C-DIC value was -18.4±0.4 ‰
548 and -14.2±1.2 ‰ for the two experiments, respectively. During the time courses of
549 the experiments, pCO_2, DIC and δ^{13}C-DIC values followed well the curves predicted
550 by the degassing model (Fig. 4).

551 First, a rapid decrease in pCO_2 occurred (from 41,160 to 9,360 ppmv and from
552 47,730 to 3,260 ppmv, for the two experiments, respectively) and in DIC (from 1,720
553 to 420 µmol L^{-1} and from 2,030 to 200 µmol L^{-1}). This first period of large and rapid
554 CO_2 degassing was associated with a moderate increase in δ^{13}C-DIC (from -26.2±0.5
555 to -24.3±0.03 ‰ and from -26.5±0.04 to -22.5±0.2 ‰). Later, slower decreases in
556 pCO_2 (from 9,360 to 530 ppmv and from 3,260 to 460 ppmv) and in DIC (from 420 to
557 55 µmol $L^{-1}$and from 200 to 90 µmol L^{-1}) occurred, associated with a large increase in
558 δ^{13}C-DIC (from -24.3±0.03 ‰ to -18.4±0.4 ‰ and from -22.5±0.2 to -14.2±1.2 ‰).
559 The general pattern of changes of δ^{13}C-DIC due to CO_2 degassing in the experiment
560 was reasonably well reproduced with our isotopic model (Fig. 4). Some experimental
561 degassing points slightly differ from theoretical curves in the lower-left part of the
562 model, where a large decrease of DIC occurs with little change in δ^{13}C-DIC (Fig. 4).
563 This could be due to less precise analysis of δ^{13}C-DIC at low DIC concentrations.

564

5. Discussion

5.1. Origin and temporal variations of DIC in groundwaters

The potential sources of DIC in groundwaters are carbonates or silicates weathering, dissolution or soil-CO_2 that originates from heterotrophic respiration of soil organic matter (SOM) and from plant root respiration. In addition, heterotrophic respiration occurs also in the saturated zone of the soil, that is, in the groundwater itself (Craft et al., 2002). Carbonate weathering produces DIC with $\delta^{13}C$ of about half of that of soil-CO_2, whereas silicates weathering produces DIC with $\delta^{13}C$ with an isotopic composition close to that of soil-CO_2 (Das et al., 2005; Wachniew, 2006; Polsenaere and Abril, 2012). Vegetation cover in the Leyre watershed is mainly C_3 plants (i.e., *Pinus pinaster*) (Govind et al., 2012). $\delta^{13}C$ of SOM that originates from C_3 plants can range between -22 and -34 ‰ (Vogel et al., 1993), with an average value of -28 ‰. The latter average stable isotopic composition of SOM is in agreement with observations of Polsenaere et al (2013) who measured at the outlet of the Leyre River, an average value for $\delta^{13}C$-POC (Particulate Organic Carbon) of -28.7±0.5 ‰ over a one year sampling. In addition, little or no fractionation occurs during mineralization of SOM (Amundson et al., 1998; Ekblad et al., 2002). However, due to selective molecular diffusion of CO_2 through the soil pores, the isotopic composition of soil-CO_2 can become enriched in ^{13}C relative to SOM by up to 4-5 ‰ (Cerling et al., 1991). Carbon isotopes are also fractionated (ε of about -1 ‰) during dissolution of soil-CO_2 into aqueous CO_2 (Zhang et al., 1995). Hence, the average $\delta^{13}C$-DIC values of -26.2±1.2 ‰ observed in groundwaters are consistent with two different sources of carbon with the same isotopic signature: (i) aqueous CO_2 derived from respiration of soil organic matter (derived from C_3 plants) in soils and groundwaters, (ii) HCO_3^- derived from weathering of silicates with soil-CO_2. Aqueous CO_2 represented 97±3 % (range is 76-100 %) of the DIC in the groundwater showing the low intensity of silicate weathering. The absence of carbonate weathering in the sampled groundwater is also consistent with the lithology of the selected stations (sands), representative for the majority of the Leyre Watershed (Fig. 1). A contribution of carbonate weathering may alter the isotopic composition of DIC in groundwaters of Miocene carbonated sands located in the most downstream of the watershed, and that were not sampled here.

During the monitoring period, seasonal changes in carbon concentration in groundwater occurred for pCO_2 and DIC but not for TA and δ^{13}C-DIC. This reveals that although the intensity of the DIC source may change over time, the origin of groundwater DIC remained the same. Lowest values of pCO_2 occurred during high flow and high groundwater table periods (Jan. 2014-Apr. 2014 and Feb. 2015-Mar. 2015), as a consequence of dilution with rainwater with low DIC content that rapidly percolates through the sand (Fig. 2a-b). Moreover, during these two wet periods, draining of groundwater is stronger, rapidly recycling the DIC present in the saturated soil, and decreasing the concentration in the groundwater. Values of pCO_2 in groundwaters start to increase at the beginning of the base flow period (May 2014 and April 2015), as a consequence of respired DOC (Dissolved Organic Carbon), that had been accumulated in groundwater because groundwater table had reached organic horizon during last high flow period (Deirmendjian, 2016). Indeed, during high flow periods (Jan. 2014-Apr 2014 and Feb. 2015-Mar. 2015), concentration of DOC in groundwater is 2,000±1,200 µmol L^{-1} whereas during base flow periods (May. 2014–Jan. 2015 and Apr. 2015–Jul. 2015) DOC concentration in groundwater is 530±160 µmol L^{-1} (Deirmendjian, 2016). During summer 2014 (Jun-Aug), values of pCO_2 in groundwaters are stable, as a consequence of no (very low) water inputs into groundwater, as attested by the decreasing groundwater table during this period (Fig. 2a-b). The second increase (27/08/14-24/09/14) of pCO_2 in groundwaters at the end of decreasing groundwater table period, could be related to a soil-CO_2 flush with the percolation of rainwater in the unsaturated soil (Johnson et al., 2008). However, at our study site, Sep. 2014 was one of the driest months throughout the sampling period (Fig. 2a), which suggests that soil-CO_2 could have been transported by simple downward diffusion. Finally, values of pCO_2 in groundwaters decrease from late summer (end of Sep. 2014) to next flood peak (Mar. 2015), as a consequence of increasing groundwater table and increasing river flow, that dilutes groundwaters and that increases drainage of groundwater, respectively.

4.2. Inorganic carbon processes affecting the isotopic signal of riverine DIC: CO_2 degassing versus carbonate weathering

In order to analyse qualitatively and quantitatively the process of CO_2 degassing and DIC isotopic equilibration with the atmosphere in streams and rivers, we have plotted δ^{13}C-DIC as a function of pCO_2, TA, and DIC (Fig. 5). The distributions of δ^{13}C-DIC versus pCO_2 followed well the trajectories predicted by the degassing model, starting in the groundwater and ending in the fourth order stream (Fig. 5a). This indicates that degassing is the dominating process that drives the spatial variations of these two parameters and that groundwater enriched in CO_2 is the main source of CO_2 in the Leyre watershed. In addition, TA is overall conservative between groundwaters, first and second order streams (Tab. 3; Fig. 2c, 3b; 5b). Consequently, changes in δ^{13}C-DIC between groundwaters and second order streams are attributable to CO_2 evasion to the atmosphere only. Furthermore, unlike in experimental degassing (Fig. 4), we never observe very high values of pCO_2 with very negative δ^{13}C-DIC (Fig. 5a) in first order streams as those found in groundwater (~-26 ‰). This suggests that CO_2 evasion between groundwaters and first order streams occurs very fast. Groundwater spring sampling and the associated large loss of pCO_2 of about 21,700±6,800 ppmv in 40 meters, confirms that degassing from groundwater is a very fast process. This conclusion is in agreement with findings of Venkiteswaran et al (2014) who mentioned that most of the CO_2 originating from groundwaters has been lost before typical in-stream sampling occurs. Thus, to improve CO_2 degassing estimation at regional and global scales (at least in lowland rivers), the value of pCO_2 in groundwaters should be taken into account in the calculation. Otherwise, the degassing flux would be probably underestimated in such environments. In the Leyre Watershed, changes in δ^{13}C-DIC between groundwaters and second order streams, are due to CO_2 degassing corresponds to an increase of 6.9±2.9 ‰ (Tab. 3; Fig. 3). As we will discuss later in section 4.3, although in-stream respiration can occur and liberate ^{13}C-depleted DIC in stream waters, its contribution to CO_2 degassing is probably minor compared to groundwater CO_2. Consequently, DIC in first and second order streams can be considered as groundwater DIC minus a large part of CO_2, which has quickly degassed.

In monolithic watersheds draining only silicate rocks, TA is typically very low, below 125 µmol L^{-1} according to Meybeck (1987). In the Leyre Watershed, although TA was below this threshold in groundwaters, and in first and second order streams, TA increased in third and fourth order streams (Tab. 3; Fig. 2c, 3b, 5b), suggesting a

significant contribution of carbonate weathering. The changes in δ^{13}C-DIC between second and fourth order stream were about 5.2±3.6 ‰ (Tab. 3; Fig. 2e; 3d; 5), from -19.3±2.7 ‰ in second order streams to -14.1±2.4 ‰ in fourth order streams. This time, the enrichment in ^{13}C is attributable not only to CO_2 evasion, as confirmed by the pCO_2 decrease (Tab. 3; Fig. 2b, 3a, 5a), but also to inputs of TA from weathering of carbonates. This increase of TA in 4th order stream is consistent with the spatial distribution of lime sand outcrops dating from Miocene Era (Fig. 1). However, the spatial distribution of superficial lime sand does not explain the increase of TA in 3rd order streams. This suggests that the increase of TA is due to deeper groundwater inputs that are in contact with lime sand layers (Legigan, 1979), consistent with the increase of TA and δ^{13}C-DIC during base flow period (Fig. 2a-c). Indeed, DIC that originates from dissolution of carbonate rocks tends to dominate as the major source of alkalinity, even in watersheds where carbonates are present only in trace amounts (Das et al 2005).

The δ^{13}C values for most carbonates of marine origin is about 0 ‰ (Clark and Fritz, 1997). Carbonates then react with soil-CO_2 and produce DIC with an isotopic composition close to the average of those of soil-CO_2 and carbonate rocks (Salomons and Mook, 1986), ie., -12 ‰ in the Leyre watershed. In order to differentiate the respective contributions of degassing and carbonate weathering between second and fourth order streams, we applied a mixing model between two DIC end-members (Fig. 5b): one end-member is DIC from second order streams and the other end-member is DIC originates from carbonate weathering with a δ^{13}C signature of -12 ‰:

$$\delta^{13}C\text{-}DIC_{mm} = ([DIC]_2 \,.\, \delta^{13}C\text{-}DIC_2 + x \,.\, \delta^{13}C\text{-}DIC_{ca})/([DIC]_2 + x) \qquad \text{(Eq. 26)}$$

Where,

$\delta^{13}C\text{-}DIC_{mm}$ is the stable isotopic composition of DIC resulting from the mixing of the two end-members; $[DIC]_2$ and $\delta^{13}C\text{-}DIC_2$ are the average composition of second order streams; $\delta^{13}C\text{-}DIC_{ca}$ is the average composition of δ^{13}C-DIC from carbonate weathering (-12 ‰); x is the fraction of DIC that originates from carbonate weathering.

This mixing model does not account for the CO_2 loss to the atmosphere and thus predicts the theoretical signature of the DIC as function of TA, when carbonate

694 weathering occurs, but CO_2 degassing does not occur. In addition, we fitted on our
695 data of δ^{13}C-DIC and TA another curve of the same form as mixing model (i.e., f(x) =
696 (A + B . x) / (C + x)), without considering a preselected value as end-member (Fig.
697 5b). δ^{13}C-DIC and TA values of second, third and fourth order streams that are above
698 the mean concentration of second order streams (i.e., δ^{13}C-DIC=-19.3 ‰ and TA=90
699 µmol L^{-1}) were used to obtain the fitted curve (Fig. 5b).

700 In the δ^{13}C-DIC versus TA plot (Fig. 5b), the fitted curve was well above that given by
701 the carbonate weathering mixing model, with a quite constant difference of -1.8 ‰.
702 This difference in δ^{13}C-DIC is attributed to CO_2 degassing between second and
703 fourth order streams, a process accounted for in the fitted curve on the experimental
704 data points, but not in the carbonate weathering mixing model. According to these
705 results, between second and fourth order streams, inputs of TA from carbonate
706 weathering increase the δ^{13}C-DIC by 3.4 ‰ whereas CO_2 degassing increase it by
707 1.8 ‰. Thus, In terms of percentages, carbonate weathering explains 65% of δ^{13}C-
708 DIC changes between second and fourth order streams whereas water-air
709 equilibration explains 35%. δ^{13}C-DIC is thus an excellent tracer of the dissolved
710 inorganic carbon processes. According to our data, transport of groundwater DIC
711 followed by degassing in streams of increasing order is the major pathway of CO_2 in
712 the Leyre watershed. Indeed, pCO_2, DIC and δ^{13}C-DIC data are explained by
713 theoretical degassing model between groundwaters and second order streams (Fig.
714 5a-c); in addition, we were also able to separate the effect of evasion on pCO_2, DIC
715 and δ^{13}C-DIC, from that of carbonate weathering on TA, DIC and δ^{13}C-DIC between
716 second and fourth order streams (Fig. 5b).

717

718 **4.3. CO_2 degassing and DIC export at the basin scale**

719 In order to estimate CO_2 degassing, we apply two independent methods at the scale
720 of the Leyre watershed. The first method consists in a mass balance calculation of
721 CO_2 at the basin scale, using water discharge and dissolved CO_2 concentrations
722 (Fig. 6); the second method consists in using average measured pCO_2 values,
723 stream surface areas, and gas transfer velocities based on hydraulic stream
724 geometric parameters (Raymond et al. 2012). For the first approach, we consider that
725 the loss of CO_2 between two different stream orders is due to rapid groundwater CO_2

evasion to the atmosphere, as attested by our degassing model that reproduced well *in situ* δ^{13}C-DIC values (Fig. 5a). We use the discharge from groundwater and upstream and the difference in CO_2* between each stream orders and the groundwater as follows:

$$F_{Or1} = Q_{Or1}(CO_2{}^*_{GW} - CO_2{}^*_{Or1}) \quad \text{(Eq. 27)}$$

$$F_{Or2} = Q_{Or1}(CO_2{}^*_{Or1} - CO_2{}^*_{Or2}) + 0.45Q_{Or2}(CO_2{}^*_{GW} - CO_2{}^*_{Or2}) \quad \text{(Eq. 28)}$$

$$F_{Or3} = Q_{Or2}(CO_2{}^*_{Or2} - CO_2{}^*_{Or3}) + 0.17Q_{Or3}(CO_2{}^*_{GW} - CO_2{}^*_{Or3}) \quad \text{(Eq. 29)}$$

$$F_{Or4} = Q_{Or3}(CO_2{}^*_{Or3} - CO_2{}^*_{Or4}) + 0.05Q_{Or4}(CO_2{}^*_{GW} - CO_2{}^*_{Or4}) \quad \text{(Eq. 30)}$$

Where,

F_{Or1}, F_{Or2}, F_{Or3} and F_{Or4}; $CO_2{}^*_{GW}$, $CO_2{}^*_{Or1}$, $CO_2{}^*_{Or2}$, $CO_2{}^*_{Or3}$ and $CO_2{}^*_{Or4}$; Q_{Or1}, Q_{Or2}, Q_{Or3} and Q_{Or4} are respectively, the degassing flux in mol s^{-1}, the concentration of aqueous-CO_2 in mol L^{-1} and the river flow L s^{-1}, in each stream order.

With this method, we find a total CO_2 degassing flux of 1.7±0.3 10^4 t C yr^{-1} (46.2±7.2 mol s^{-1}) from the watershed, first and second order streams accounting respectively for 40 % and 36 % of the total (Tab. 4; Fig. 6); In addition, it is important to note that the diffusive inputs of groundwaters in each stream orders are significant in the budget. Indeed, if we assumed that all the discharge measured at the watershed outlet (fourth stream order) was originating from first order streams (assuming discharge is conservative and groundwater inputs in second, third and fourth order streams are negligible), the total flux of CO_2 evasion in the Leyre watershed would be the same, but the contribution of first order streams would be more than 90% (compared to 40% here).

The second method is based on the stream surface area, the water-air gradient and the gas transfer velocity. Stream hydraulic parameters (W, D, V) modelled with empirical equations from Raymond et al. (2012) were relatively consistent with field measurements at the sampling stations (Tab. 1), which suggests that the calculated k_{600} are robust. This second method gave a total degassing flux of 1.5±0.5 10^4 t C yr^{-1} (38.5±14.1 mol s^{-1}), that is 20% lower than method 1.

CO_2 degassing fluxes and k_{600} values obtained with the two independent methods were very consistent for stream orders 2, 3 and 4, but fluxes from the hydrological mass balance (method 1) were 75% higher for first order streams. This suggests that

in very small streams, the method based on surface area and gas transfer velocity (method 2) may underestimate outgassing. This could be due to the hotspot character of CO_2 evasion and the very fast degassing at the groundwater-stream interface that cannot be apprehended with conventional stream sampling. This hypothesis was confirmed by our observations in spring water that loosed 70% of their CO_2 40 meters downstream.

Another important question that must be carefully considered when comparing the two methods is the contribution of in-stream respiration to outgassing. Indeed, method 1 based on mass balance calculation assumes that all the CO_2 originates from the groundwater, whereas method 2 based on gas transfer velocity accounts for all the CO_2 outgassed from the streams: the CO_2 from the groundwater and the CO_2 produced by in-stream net heterotrophy (Battin et al., 2008; Hotchkiss et al., 2015). The fact that method 1 (that neglects in-stream respiration) gives a CO_2 outgassing flux higher than that with method 2 suggests that in-stream heterotrophy is within the uncertainty of the two methods and a minor component of CO_2 outgassing in the Leyre watershed. In their analysis on rivers of different size Hotchkiss et al (2015), reported an average contribution of in-stream net heterotrophy of 14% the CO_2 degassing of US streams with discharges of less than 0.01 $m^3 s^{-1}$. In the case of the Leyre river basin, measurements of metabolic activity in very shallow water depths of first order streams are missing. In addition, a significant part of the in-stream respiration may be benthic, using litter from riparian vegetation.

In order to close a DIC budget of the Leyre watershed (Tab.5, Fig. 6), we also calculated the export of C to the Arcachon Lagoon at the most downstream gauging stations using mean DIC concentration and mean river flow in fourth order stream. As pCO_2 at this downstream station was still far from the equilibrium with the atmosphere, 18% the DIC input to the coastal lagoon was in the form of Excess CO_2. Excess CO_2 as defined as the quantity of DIC that is transferred as CO_2 to the atmosphere after complete water-air equilibration (Abril et al., 2000) was calculated as the difference between in-situ DIC (i.e., calculated with in situ TA, pCO_2 and

789 temperature) and a theoretical calculated DIC at equilibrium with the atmosphere
790 (400 ppmv). Excess CO_2 will be rapidly degassed in the Arcachon lagoon. In total,
791 the terrestrial ecosystem in the Leyre watershed exports on average 54.3±29.3 mol s^{-1}
792 as DIC to surface waters. Among this total flux, 85% returns to the atmosphere from
793 the stream surface as CO_2, 3% potentially degases in the Arcachon lagoon and 12%
794 is exported as alkalinity to the coastal ocean (Table 5).

795

796

797 **IV.5.Conclusion**

798 The isotopic composition of the DIC in groundwaters and streams indicates that
799 the primary control on carbon fluxes in first and second order streams is degassing of
800 groundwater CO_2 resulting from soil respiration. In third and fourth order streams,
801 carbonates weathering also contribute to the ^{13}C enrichment of DIC downstream. Our
802 DIC, TA and $\delta^{13}C$-DIC data allowed us to quantify the relative importance of gas
803 exchange and carbonates weathering along the river course with increasing stream
804 orders. In order to calculate a CO_2 mass balance of the Leyre watershed, we used a
805 classical method based on stream hydrology and geometry, water pCO_2, surface
806 area, and gas transfer velocity. We compared this method with a hydrological method
807 that calculates the loss of dissolved CO_2 between groundwater and each stream
808 order, using concentrations and drainage factors. The two methods give consistent
809 results except in first order streams were the method based on water pCO_2 and gas
810 transfer velocity apparently missed some CO_2 emission hotspots in headwaters.
811 Evasion of CO_2 from first and second order streams was the dominant component of
812 the entire DIC flux in the watershed, accounting for about 75 % of the total CO_2
813 evasion flux from river network. Overall, CO_2 evasion from river system represents
814 85% of the entire DIC export from the Leyre watershed, the remaining part being
815 alkalinity (mainly from carbonates weathering downstream) and some Excess CO_2
816 that are exported to the Arcachon Lagoon.

817

818 **Acknowledgments**

819 This research is part of the CNP-Leyre project funded by the Cluster of
820 Excellence COTE at the Université de Bordeaux (ANR-10-LABX-45). We thank

Dominique Poirier, Luiz Carlos Cotovicz Junior, Katixa Lajaunie-Salla, Baptiste Voltz, Gwenaëlle Chaillou and Damien Buquet (EPOC Bordeaux) for their assistance in the field. Karine Charlier and Céline Charbonnier helped with chemical and isotopic analysis; Christophe Chipeaux and Denis Loustau (ISPA, INRA Bordeaux) provided water table data and Bernard Gaillard (DIREN Aquitaine) provided river discharge chronic.

References

Abril, G., Bouillon, S., Darchambeau, F., Teodoru, C.R., Marwick, T.R., Tamooh, F., Ochieng Omengo, F., Geeraert, N., Deirmendjian, L., Polsenaere, P., Borges, A.V., 2015. Technical Note: Large overestimation of pCO2 calculated from pH and alkalinity in acidic, organic-rich freshwaters. Biogeosciences 12, 67–78. doi:10.5194/bg-12-67-2015

Abril, G., Etcheber, H., Borges, A.V., Frankignoulle, M., 2000. Excess atmospheric carbon dioxide transported by rivers into the Scheldt estuary. Comptes Rendus de l'Academie des Sciences-Series IIA-Earth and Planetary Science 330, 761–768.

Acuña, V., Giorgi, A., Muñoz, I., Uehlinger, U.R.S., Sabater, S., 2004. Flow extremes and benthic organic matter shape the metabolism of a headwater Mediterranean stream. Freshwater Biology 49, 960–971.

Amiotte-Suchet, P., Probst, J.-L., Ludwig, W., 2003. Worldwide distribution of continental rock lithology: Implications for the atmospheric/soil CO2 uptake by continental weathering and alkalinity river transport to the oceans. Global Biogeochemical Cycles 17.

Amundson, R., Stern, L., Baisden, T., Wang, Y., 1998. The isotopic composition of soil and soil-respired CO 2. Geoderma 82, 83–114.

Augusto, L., Bakker, M.R., Morel, C., Meredieu, C., Trichet, P., Badeau, V., Arrouays, D., Plassard, C., Achat, D.L., Gallet-Budynek, A., Merzeau, D., Canteloup, D., Najar, M., Ranger, J., 2010. Is "grey literature" a reliable source of data to characterize soils at the scale of a region? A case study in a maritime pine forest in southwestern France. European Journal of Soil Science 61, 807–822. doi:10.1111/j.1365-2389.2010.01286.x

Battin, T.J., Kaplan, L.A., Findlay, S., Hopkinson, C.S., Marti, E., Packman, A.I., Newbold, J.D., Sabater, F., 2008. Biophysical controls on organic carbon fluxes in fluvial networks. Nature Geosci 2, 595–595. doi:10.1038/ngeo602

Borges, A.V., 2005. Do we have enough pieces of the jigsaw to integrate CO2 fluxes in the coastal ocean? Estuaries 28, 3–27.

Bott, T.L., Montgomery, D.S., Newbold, J.D., Arscott, D.B., Dow, C.L., Aufdenkampe, A.K., Jackson, J.K., Kaplan, L.A., 2006. Ecosystem metabolism in streams of the Catskill mountains (Delaware and Hudson river watersheds) and lower Hudson valley. Journal of the North American Benthological Society 25, 1018–1044.

Brunet, F., Gaiero, D., Probst, J.-L., Depetris, P.J., Gauthier Lafaye, F., Stille, P., 2005. δ13C tracing of dissolved inorganic carbon sources in Patagonian rivers (Argentina). Hydrological Processes 19, 3321–3344.

Butman, D., Raymond, P.A., 2011. Significant efflux of carbon dioxide from streams and rivers in the United States. Nature Geosci 4, 839–842. doi:10.1038/ngeo1294

Cai, W.-J., Guo, X., Chen, C.-T.A., Dai, M., Zhang, L., Zhai, W., Lohrenz, S.E., Yin, K., Harrison, P.J., Wang, Y., 2008. A comparative overview of weathering intensity and HCO 3- flux in the world's major rivers with emphasis on the

874 Changjiang, Huanghe, Zhujiang (Pearl) and Mississippi Rivers. Continental
875 Shelf Research 28, 1538–1549.

876 Cerling, T.E., Solomon, D.K., Quade, J., Bowman, J.R., 1991. On the isotopic
877 composition of carbon in soil carbon dioxide. Geochimica et Cosmochimica
878 Acta 55, 3403–3405.

879 Ciais, P., Sabine, C., Bala, G., Bopp, L., Brovkin, V., Canadell, J., Chhabra, A.,
880 DeFries, R., Galloway, J., Heimann, M., Jones, C., Le Quéré, C., Myeni, R..,
881 Piao, S., Thornton, P., 2013. Carbon and other biogeochemical cycles, in:
882 Climate Change 2013: The Physical Science Basis. Contribution of Working
883 Group I to the Fifth Assessment Report of the Intergovernmental Panel on
884 Climate Change. Cambridge University Press, Cambridge, United Kingdom
885 and New York, NY, USA., pp. 465–570.

886 Clark, I., Fritz, P., 1997. Environmental isotopes in hydrology. Lewis Publishers, Boca
887 Raton, Fla.

888 Cole, J.J., Caraco, N.F., 2001. Carbon in catchments: connecting terrestrial carbon
889 losses with aquatic metabolism. Mar. Freshwater Res. 52, 101–110.

890 Cole, J.J., Prairie, Y.T., Caraco, N.F., McDowell, W.H., Tranvik, L.J., Striegl, R.G.,
891 Duarte, C.M., Kortelainen, P., Downing, J.A., Middelburg, J.J., Melack, J.,
892 2007. Plumbing the Global Carbon Cycle: Integrating Inland Waters into the
893 Terrestrial Carbon Budget. Ecosystems 10, 171–184. doi:10.1007/s10021-
894 006-9013-8

895 Corbier, P., Karnay, G., Bourgine, B., Saltel, M., 2010. Gestion des eaux souterraines
896 en région Aquitaine. Reconnaissance des potentialités aquiferes du Mio-Plio-
897 Quaternaire des Landes de Gascogne et du Médoc en relation avec les
898 SAGE. No. Rapport final, BRGM RP 57813.

899 Craft, J.A., Stanford, J.A., Pusch, M., 2002. Microbial respiration within a floodplain
900 aquifer of a large gravel-bed river. Freshwater Biology 47, 251–261.

901 Das, A., Krishnaswami, S., Bhattacharya, S.K., 2005. Carbon isotope ratio of
902 dissolved inorganic carbon (DIC) in rivers draining the Deccan Traps, India:
903 sources of DIC and their magnitudes. Earth and Planetary Science Letters
904 236, 419–429.

905 Davidson, E.A., Figueiredo, R.O., Markewitz, D., Aufdenkampe, A.K., 2010.
906 Dissolved CO2 in small catchment streams of eastern Amazonia: A minor
907 pathway of terrestrial carbon loss. Journal of Geophysical Research:
908 Biogeosciences 115.

909 Deirmendjian, L., 2016. Transfert de carbone le long du continuum végétation-sol-
910 nappe-rivière-atmosphère dans le bassin de la Leyre (Landes de gascogne,
911 SO France). Université de Bordeaux.

912 Doctor, D.H., Kendall, C., Sebestyen, S.D., Shanley, J.B., Ohte, N., Boyer, E.W.,
913 2008. Carbon isotope fractionation of dissolved inorganic carbon (DIC) due to
914 outgassing of carbon dioxide from a headwater stream. Hydrological
915 Processes 22, 2410–2423.

916 Ekblad, A., Nyberg, G., Högberg, P., 2002. 13C-discrimination during microbial
917 respiration of added C3-, C4-and 13C-labelled sugars to a C3-forest soil.
918 Oecologia 131, 245–249.

Frankignoulle, M., Borges, A.V., 2001. Direct and Indirect pCO2 Measurements in a Wide Range of pCO2 and Salinity Values (The Scheldt Estuary). Aquatic Geochemistry 7, 267–273. doi:10.1023/A:1015251010481

Frankignoulle, M., Bourge, I., Wollast, R., 1996. Atmospheric CO2 fluxes in a highly polluted estuary (the Scheldt). Limnology and Oceanography.

Gillikin, D.P., Bouillon, S., 2007. Determination of δ18O of water and δ13C of dissolved inorganic carbon using a simple modification of an elemental analyser-isotope ratio mass spectrometer: an evaluation. Rapid Communications in Mass Spectrometry 21, 1475–1478.

Govind, A., Bonnefond, J.-M., Kumari, J., Moisy, C., Loustau, D., Wigneron, J.-P., 2012. Modeling the ecohydrological processes in the Landes de Gascogne, SW France, in: Plant Growth Modeling, Simulation, Visualization and Applications (PMA), 2012 IEEE Fourth International Symposium on. IEEE, pp. 133–140.

Gran, G., 1952. Determination of the equivalence point in potentiometric titrations of seawater with hydrochloric acid. Oceanol. Acta 5, 209–218.

Hotchkiss, E.R., Hall Jr, R.O., Sponseller, R.A., Butman, D., Klaminder, J., Laudon, H., Rosvall, M., Karlsson, J., 2015. Sources of and processes controlling CO2 emissions change with the size of streams and rivers. Nature Geoscience 8, 696–699.

Johnson, M.S., Lehmann, J., Riha, S.J., Krusche, A.V., Richey, J.E., Ometto, J.P.H., Couto, E.G., 2008. CO2 efflux from Amazonian headwater streams represents a significant fate for deep soil respiration. Geophysical Research Letters 35.

Jolivet, C., Augusto, L., Trichet, P., Arrouays, D., 2007. Forest soils in the Gascony Landes Region: formation, history, properties and spatial varaibility [WWW Document]. URL http://hdl.handle.net/2042/8480

Keeling, C.D., Carter, A.F., Mook, W.G., 1984. Seasonal, latitudinal, and secular variations in the abundance and isotopic ratios of atmospheric CO2: 2. Results from oceanographic cruises in the tropical Pacific Ocean. Journal of Geophysical Research: Atmospheres (1984–2012) 89, 4615–4628.

Kokic, J., Wallin, M.B., Chmiel, H.E., Denfeld, B.A., Sobek, S., 2015. Carbon dioxide evasion from headwater systems strongly contributes to the total export of carbon from a small boreal lake catchment. Journal of Geophysical Research: Biogeosciences 120, 2014JG002706. doi:10.1002/2014JG002706

Lauerwald, R., Hartmann, J., Moosdorf, N., Kempe, S., Raymond, P.A., 2013. What controls the spatial patterns of the riverine carbonate system?—A case study for North America. Chemical geology 337, 114–127.

Legigan, P., 1979. L'élaboration de la formation du sable des Landes, dépôt résiduel de l'environnement sédimentaire pliocène-pléïstocène centre aquitain. Institut de géologie du Bassin d'Aquitaine.

Martin, J.-M., Meybeck, M., 1979. Elemental mass-balance of material carried by major world rivers. Marine chemistry 7, 173–206.

Meybeck, M., 1987. Global chemical weathering of surficial rocks estimated from river dissolved loads. American Journal of Science 401–428.

963 Meybeck, M., 1982. Carbon, nitrogen, and phosphorus transport by world rivers. Am.
964 J. Sci 282, 401–450.

965 Meybeck, M., 1981. River transport of organic carbon to the ocean. NAS-NRC
966 Carbon Dioxide Effects Res. and Assessment Program: Flux of Org. Carbon
967 by Rivers to the Oceans p 219-269(SEE N 81-30674 21-45).

968 Millero, F.J., 1979. The thermodynamics of the carbonate system in seawater.
969 Geochimica et Cosmochimica Acta 43, 1651–1661.

970 Miyajima, T., Miyajima, Y., Hanba, Y.T., Yoshii, K., Koitabashi, T., Wada, E., 1995.
971 Determining the stable isotope ratio of total dissolved inorganic carbon in lake
972 water by GC/C/IIRMS. Limnology and Oceanography 40, 994–1000.

973 Moreaux, V., Lamaud, É., Bosc, A., Bonnefond, J.-M., Medlyn, B.E., Loustau, D.,
974 2011. Paired comparison of water, energy and carbon exchanges over two
975 young maritime pine stands (Pinus pinaster Ait.): effects of thinning and
976 weeding in the early stage of tree growth. Tree physiology tpr048.

977 Polsenaere, P., Abril, G., 2012. Modelling CO2 degassing from small acidic rivers
978 using water pCO2, DIC and δ13C-DIC data. Geochimica et Cosmochimica
979 Acta 91, 220–239. doi:10.1016/j.gca.2012.05.030

980 Polsenaere, P., Savoye, N., Etcheber, H., Canton, M., Poirier, D., Bouillon, S., Abril,
981 G., 2013a. Export and degassing of terrestrial carbon through watercourses
982 draining a temperate podzolized catchment. Aquatic sciences 75, 299–319.

983 Polsenaere, P., Savoye, N., Etcheber, H., Canton, M., Poirier, D., Bouillon, S., Abril,
984 G., 2013b. Export and degassing of terrestrial carbon through watercourses
985 draining a temperate podzolized catchment. Aquatic sciences 75, 299–319.

986 Raymond, P.A., Hartmann, J., Lauerwald, R., Sobek, S., McDonald, C., Hoover, M.,
987 Butman, D., Striegl, R., Mayorga, E., Humborg, C., Kortelainen, P., Dürr, H.,
988 Meybeck, M., Ciais, P., Guth, P., 2013. Global carbon dioxide emissions from
989 inland waters. Nature 503, 355–359. doi:10.1038/nature12760

990 Raymond, P.A., Zappa, C.J., Butman, D., Bott, T.L., Potter, J., Mulholland, P.,
991 Laursen, A.E., McDowell, W.H., Newbold, D., 2012. Scaling the gas transfer
992 velocity and hydraulic geometry in streams and small rivers. Limnology and
993 Oceanography: Fluids and Environments 2, 41–53.

994 Riley, A.J., Dodds, W.K., 2013. Whole-stream metabolism: strategies for measuring
995 and modeling diel trends of dissolved oxygen. Freshwater Science 32, 56–69.
996 doi:10.1899/12-058.1

997 Salomons, W., Mook, W.G., 1986. Isotope geochemistry of carbonates in the
998 weathering zone. Handbook of environmental isotope geochemistry 2, 239–
999 269.

1000 Venkiteswaran, J.J., Schiff, S.L., Wallin, M.B., 2014. Large Carbon Dioxide Fluxes
1001 from Headwater Boreal and Sub-Boreal Streams. PLoS ONE 9, e101756.
1002 doi:10.1371/journal.pone.0101756

1003 Vidon, P., Allan, C., Burns, D., Duval, T.P., Gurwick, N., Inamdar, S., Lowrance, R.,
1004 Okay, J., Scott, D., Sebestyen, S., 2010. Hot spots and hot moments in
1005 riparian zones: Potential for improved water quality management1. Wiley
1006 Online Library.

1007 Vogel, J.C., Ehleringer, J.R., Hall, A.E., Farquhar, G.D., 1993. Variability of carbon
1008 isotope fractionation during photosynthesis., in: Stable Isotopes and Plant
1009 Carbon-Water Relations. Academic Press Inc., pp. 29–46.

1010 Wachniew, P., 2006. Isotopic composition of dissolved inorganic carbon in a large
1011 polluted river: The Vistula, Poland. Chemical Geology 233, 293–308.

1012 Wallin, M.B., Grabs, T., Buffam, I., Laudon, H., Ågren, A., Öquist, M.G., Bishop, K.,
1013 2013. Evasion of CO2 from streams – The dominant component of the carbon
1014 export through the aquatic conduit in a boreal landscape. Glob Change Biol
1015 19, 785–797. doi:10.1111/gcb.12083

1016 Weiss, R., 1974. Carbon dioxide in water and seawater: the solubility of a non-ideal
1017 gas. Marine chemistry 2, 203–215.

1018 Zappa, C.J., McGillis, W.R., Raymond, P.A., Edson, J.B., Hintsa, E.J., Zemmelink,
1019 H.J., Dacey, J.W., Ho, D.T., 2007. Environmental turbulent mixing controls on
1020 air-water gas exchange in marine and aquatic systems. Geophysical Research
1021 Letters 34.

1022 Zhang, J., Quay, P.D., Wilbur, D.O., 1995. Carbon isotope fractionation during gas-
1023 water exchange and dissolution of CO 2. Geochimica et Cosmochimica Acta
1024 59, 107–114.

1025

1026

Stream orders	0*	1	2	3	4
Number of streams in the whole watershed[a]		619	69	2	1
Cumulated river length for the whole watershed[a] (km)		1,610	750	115	40
Cumulated river flow[b] (m^3 s^{-1})		9.2±2.6	16.8±5.0	20.2±2.8	21.3
Mean river flow[c] (m^3 s^{-1})		0.01±0.004	0.24±0.07	10.1±1.4	21.3
Depth[d] (m)		0.12±0.03	0.27±0.08	0.78±0.11	0.97±0.14
Width[d] (m)		2.2±0.6	7.1±2.1	34.0±4.8	46.5±6.5
Velocity[d] (m s^{-1})		0.05±0.02	0.12±0.04	0.37±0.05	0.46±0.06
Water surface area[e] (km^2)		3.5±1.0	5.3±1.6	3.9±0.5	1.9±0.3
Slope[f] (%)		0.310±0.28	0.23±0.14	0.11	0.04
k_{600}[g] (m d^{-1})		1.2±0.6	1.9±0.4	3.4±0.8	2.1±0.5
Number of the studied stations	3	6	6	4	2
River width of the studied stations[h] (m)		1.7±1.2	5.2±2.4	15±5.5	31±10.8
River length of the studied stations[i] (km)		2.6±1.4	10.8±4.6	57.5±7.5	40
Forest occupation of the studied stations[j] (%)	100	96±3	86±3	83±2	84±0.4
Catchment surface area of the studied stations[k] (km^2)		15±13	98±40	446±99	1,863±240
Number of gauging stations[l]		0	2	1	1
Depth of the gauging stations[m] (m)		0.13±0.01	0.32±0.16	0.72±0.32	1.14±0.85
Water velocity[n] (m s^{-1})		0.10±0.08			

Table 1: Characteristics of the Leyre watershed and sampling network. * order zero corresponds to groundwater. [a, i] calculated from BD CARTHAGE ®. [b]estimated from our hydrological model and from the mean river flow of 21.3 m^3 s^{-1} during the sampling period (Tab. 2). [c]Mean river flow (Q_{mean}) is determined with the cumulated river flow and the number of streams per stream orders. [d]estimated using hydraulic equations from Raymond et al (2012). [e]estimated from cumulated river length and mean width per stream orders. [f, k]estimated from ArcGIS 10.2 (spatial analyst extension). [g]estimated as the average (±SD) gas transfer velocity given by the 7 quations of Raymond et al (2012). [h]estimated from field measurements (decameter or laser rangefinder).[j]estimated with corine

land cover 2006. [l]Gauging stations are included in the number of the studied stations. [m]estimated from the French water agency database over the 2014-2015 period in second, third and fourth order stream; estimated from field measurements in first order streams (in headwater's spring and in a larger first order stream). [n]estimated from field measurements (in headwater's spring and in a larger first order stream).

Stream order			Order 2		Order 3		Order 4
Gauging stations			GAR	BR	PL		GL
2014-2015	Q (m^3 s^{-1})		0.4±0.5	1.0±1.3	3.5±3.7		17.9±20.4
	Dr (m^3 km^{-2} s^{-1})		765±970	920±1,340	855±920		940±1,070
	α (unitless)				1.41±0.45*	0.98±0.28**	1.05±0.15
		Order 1	Order 2				
01/04/2015	Q_1	0.305	1.29	0.435			
	Dr_1	773	995	1,140			
	α_1		1.29	1.48			
	Q_2	0.276	1.29	0.435			
	Dr_2	732	995	1,140			
	α_2		1.36	1.56			
22/02/2016	Q_3	0.304	2.30	0.487			
	Dr_3	771	1,774	1,275			
	α_3		2.30	1.65			
	Q_4	0.233	2.30	0.487			
	Dr_4	610	1,774	1,275			
	α_4		2.91	2.09			
Hydrological model	α_{mean}		1.83±0.53		1.20±0.36		1.05±0.15
	% of groundwater	100%	45 %		17 %		5 %

Table 2: Hydrological model of the Leyre watershed. Q is the mean daily (±SD) river flow during the 2014-2015 period. Dr is the mean daily (±SD) drainage factor (i.e., discharge divided by the catchment area) during the 2014-2015 period. α is the ratio between two drainages of two streams of successive orders. *compared to the Grand Arriou (GAR) stream (catchment area = 112 km², slope = 0.24%). **compared to the Bourron (BR) stream (catchment area = 33 km², slope = 0.47%). Q_1, Q_2, Q_3, Q_4 correspond to the discharge of the four river flow measurements in first order streams as well as the discharge of the GAR and the BR the same day. Dr_1, Dr_2, Dr_3 and Dr_4 and. α_1, α_2, α_3 and α_4 are the corresponding drainage factors and drainage ratios, respectively. α_{mean} correspond to the mean increase of drainage ratio between streams of successive orders. For example, in second order streams α_{Order2}= 1.83±0.53α_{Order1} means that

Q_{Order2}=1.83±0.53Q_{Order1} and that diffusive groundwater inputs in second order streams represented 45% of their water discharge while the 55% remaining is coming from first order streams.

	T (°C)	pH	Conductivity (µS m^{-1})	pCO_2 (ppmv)	TA (µmol L^{-1})	DIC (µmol L^{-1})	δ^{13}C-DIC (‰)
Groundwater	**13.5±2.2**	**4.5±0.2**	**113±45**	**48,070±26,320**	**71±25**	**2,300±1,120**	**-26.2±1.2**
	[8.5~17.9]	[3.7~4.8]	[67~268]	[7,680~116,380]	[32~135]	[570~5,370]	[-28.8~-23.4]
First order	**12.9±4**	**5.9±0.4**	**116±28**	**4,820±4,540**	**74±45**	**310±210**	**-19.8±2.7**
	[4.8~22.1]	[5.1~6.9]	[72~187]	[1,010~27,205]	[29~280]	[87~1,280]	[-27.6~-12.4]
Second order	**12.8±2.7**	**6.1±0.5**	**120±35**	**3,000±1,090**	**90±60**	**240±65**	**-19.3±2.7**
	[6.3~18.3]	[4.6~6.9]	[62~256]	[1,445~6,430]	[30~410]	[140~545]	[-27.4~-13.5]
Third order	**13.4±3.1**	**6.6±0.5**	**130±20**	**1,740±580**	**230±190**	**310±180**	**-16.2±4.4**
	[7.8~19.5]	[5.5~7.5]	[83~180]	[1,058~3,271]	[35~715]	[120~780]	[-35.4~-11.5]
Fourth order	**13.6±3**	**6.8±0.3**	**150±20**	**1,740±460**	**300±110**	**380±100**	**-14.1±2.4**
	[9~18.4]	[5.9~7.3]	[81~198]	[1,163~2,925]	[60~500]	[140~580]	[-21.1~-11.9]

Table 3: Spatial distribution of dissolved inorganic carbon and ancillary parameters in the Leyre watershed throughout the sampling period (Jan. 2014-Jul. 2015); Average±SD are shown in bold (averaged value at different stations with same stream order) and range are shown between brackets (range of all stations with same stream order).

Stream Orders	1st	2nd	3rd	4th
Method 1				
Water discharge (m^3 s^{-1})				
From groundwater	9.2±2.6	7.6±2.1	3.4±1.0	1.1±0.1
From upstream	0	9.2±2.6	16.8±5.0	20.2±2.8
Total	9.2±2.6	16.8±5.0	20.2±2.8	21.3
ΔCO_2^* (µmol L^{-1})				
With groundwater	2,018	2,110	2,171	2,172
With upstream		91	62	1
CO_2^* degassing flux (mol s^{-1})				
From groundwater	18.6±5.2	15.9±4.5	7.5±2.2	2.3±0.3
From upstream	0	0.9±0.2	1.0±0.3	0.02±0.002
Total	18.6±5.2	16.8±4.5	8.5±2.3	2.3±0.3
Contribution to the total (%)	40	36	18	6
Aerial CO_2 flux[a] (µmol m^{-2} s^{-1})	5.3±2.1	3.1±1.3	2.2±0.7	1.3±0.2
k[b] (m d^{-1})	2.1±2.0	2.2±1.1	2.9±1.3	1.7±0.6
k_{600} (m d^{-1})	2.5±2.4	2.5±1.3	3.5±1.5	2.0±0.7
Method 2				
Surface area	3.5±1.0	5.3±1.6	3.9±0.5	1.9±0.3
ΔpCO_2 (µatm)	4,420	2,600	1,340	1,340
k_{600}[c] (m d^{-1})	1.2±0.6	1.9±0.4	3.4±0.8	2.1±0.5
Aerial CO_2 flux (µmol m^{-2} s^{-1})	3.0±1.1	2.8±0.6	2.5±0.5	1.5±0.5
CO_2^* degassing flux (mol s^{-1})	10.6±10.5	15.1±7.6	9.9±4.2	2.8±1.2
Contribution to the total (%)	28	39	26	7

Table 4: Water discharge and degassing CO_2 fluxes in each stream order in the Leyre Watershed. [a]calculated as the flux divided by the surface area of water. [b]for method 1, k was calculated as the degassing flux divided by the water stream area and the water-air gradient (with $pCO_{2\ air}$ =

400 ppmv).[c] for method 2, k_{600} was calculated as the average (±SD) of values given by the 7 empirical equations proposed by Raymond et al. (2012) as function of discharge, slope, velocity, and/or depth.

		mol s^{-1}	g C m^{-2} yr^{-1}	% of total
CO_2 outgassing from streams	1st order	18.6±5.2	3.4±0.9	34
	2nd order	16.8±4.5	3.0±0.8	31
	3rd order	8.5±2.3	1.5±0.4	16
	4th order	2.3±0.3	0.4±0.06	4
	Sub-Total	46.2±7.2	8.3±1.3	85
DIC Export as excess CO_2 to coastal ocean		1.4±0.5	0.25±0.01	3
DIC Export at the atmospheric equilibrium to coastal ocean		6.7±2.5	1.2±0.5	12
Total DIC export from the watershed		54.3±29.3	9.8±5.3	100%

1054 Table 5: DIC budget of the Leyre watershed. Fluxes are given as absolute numbers (mol s^{-1}) or as normalized to the surface area of the entire watershed (g C
1055 m^{-2} yr^{-1}).

1056

1057

1058

Figure 1: Map of the Leyre watershed showing the river network, the lithology and the locations of groundwater and surface waters sampling and gauging stations and their associated sub-watersheds. Gauging stations are all also sampling stations. GL, PL, GAR, BR are respectively the Grande Leyre, the Petite Leyre, the Grand Arriou, the Bourron gauging stations of the French water agency.

Figure 2: Seasonal variations of hydrology and inorganic carbon speciation and isotopic composition in the different river orders. (a) Daily discharge of the Leyre River at the outlet, groundwater table at the Bilos station and monthly precipitation at Belin-Beliet municipality, (b) partial pressure of carbon dioxide (pCO_2), (c) total alkalinity (TA), (d) dissolved inorganic carbon (DIC), (e) stable isotopic composition of DIC (δ^{13}C-DIC). Each point represents the mean value obtained at different stations with same stream order (spatial average), and the error bars correspond to the Pearson standard deviation (spatial heterogeneity). Grey side bar represents high flow periods

Figure 3: Spatial variations of dissolved inorganic carbon species in the Leyre watershed during the study period according to stream order. (a) Partial pressure of carbon dioxide (pCO_2), (b) total alkalinity (TA), (c) dissolved inorganic carbon (DIC), (d) stable isotope composition of DIC (δ^{13}C-DIC). Box-plots represent the mean (red bar), the median (black bar) as well as 10^{th}, 25^{th}, 75^{th} and 95^{th} percentile. A black square indicates that data were significantly different from those immediately at their left with $p<0.001$. A white square indicate that data were significantly different from those immediately at their left with $p<0.05$.

Figure 4: Isotopic equilibration of DIC during experimental degassing. Results of the two degassing experiments, showing the evolution of pCO_2, DIC and δ^{13}C-DIC. The continuous lines show the theoretical degassing model. Note that total alkalinity (TA) was constant during the experiments**.**

Figure 5: Stable isotopic composition of DIC (δ^{13}C-DIC) plotted against pCO_2 (a), TA (b) and DIC (c) for groundwaters and each stream orders. Empty symbols correspond to high flow samples whereas full symbols correspond to base flow samples. Larger symbols with error bars correspond to the average±SD (standard deviation) in each stream order throughout sampling period. Curves in panel (a) and (c), represent modeled changes in δ^{13}C-DIC considering only the loss of CO_2 by degassing from stream water to the atmosphere; the theoretical model was applied using a TA value of 72 µmol L^{-1} (dashed line), which corresponds to the mean concentration in groundwaters and a value of 296 µmol L^{-1} (solid line), which corresponds to the mean concentration in fourth order streams. Curves in panel (b), represent a mixing model (dash line) for the contribution of carbonate weathering and a mixing model (solid line) fitted to the dataset in second, third and fourth order streams above the mean signal of second order stream (TA=90 µmol L^{-1}, δ^{13}C-DIC=-19.3 ‰).

Figure 6: Mass balance of DIC along the groundwater-stream-atmosphere continuum in the Leyre Watershed during the monitoring period (Jan. 2014-Jul. 2015). Black arrows and black numbers represent water fluxes in m^3 s^{-1}. Red arrows and red numbers represent DIC fluxes in mol s^{-1}. Orange arrows and orange numbers represent dissolved CO_2 fluxes in mol s^{-1}. Blue arrows and blue numbers represent atmospheric CO_2 fluxes in mol s^{-1}. The export of DIC and excess CO_2 between each boxes are calculated from the mean concentration during the monitoring period (Jan. 2014-Jul. 2015) and the corresponding water flux. The degassing flux in blue is calculated following the equations 27, 28, 29 and 30.

1108

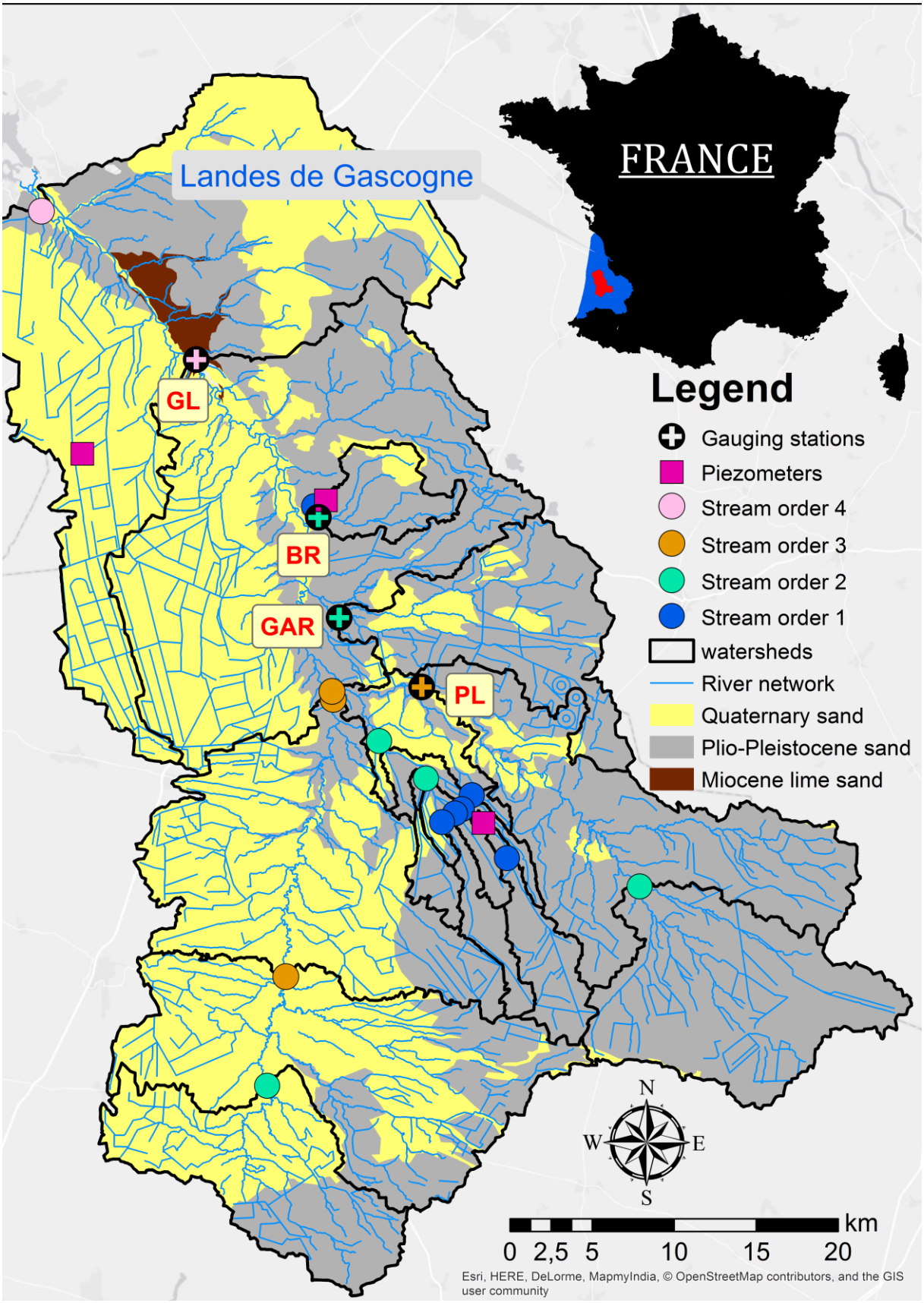
Landes de Gascogne
FRANCE
GL
BR
GAR
PL
Legend
Gauging stations
Piezometers
Stream order 4
Stream order 3
Stream order 2
Stream order 1
watersheds
River network
Quaternary sand
Plio-Pleistocene sand
Miocene lime sand
N
W
E
S
km
0 2,5 5 10 15 20
Esri, HERE, DeLorme, MapmyIndia, © OpenStreetMap contributors, and the GIS user community

FIGURE 1

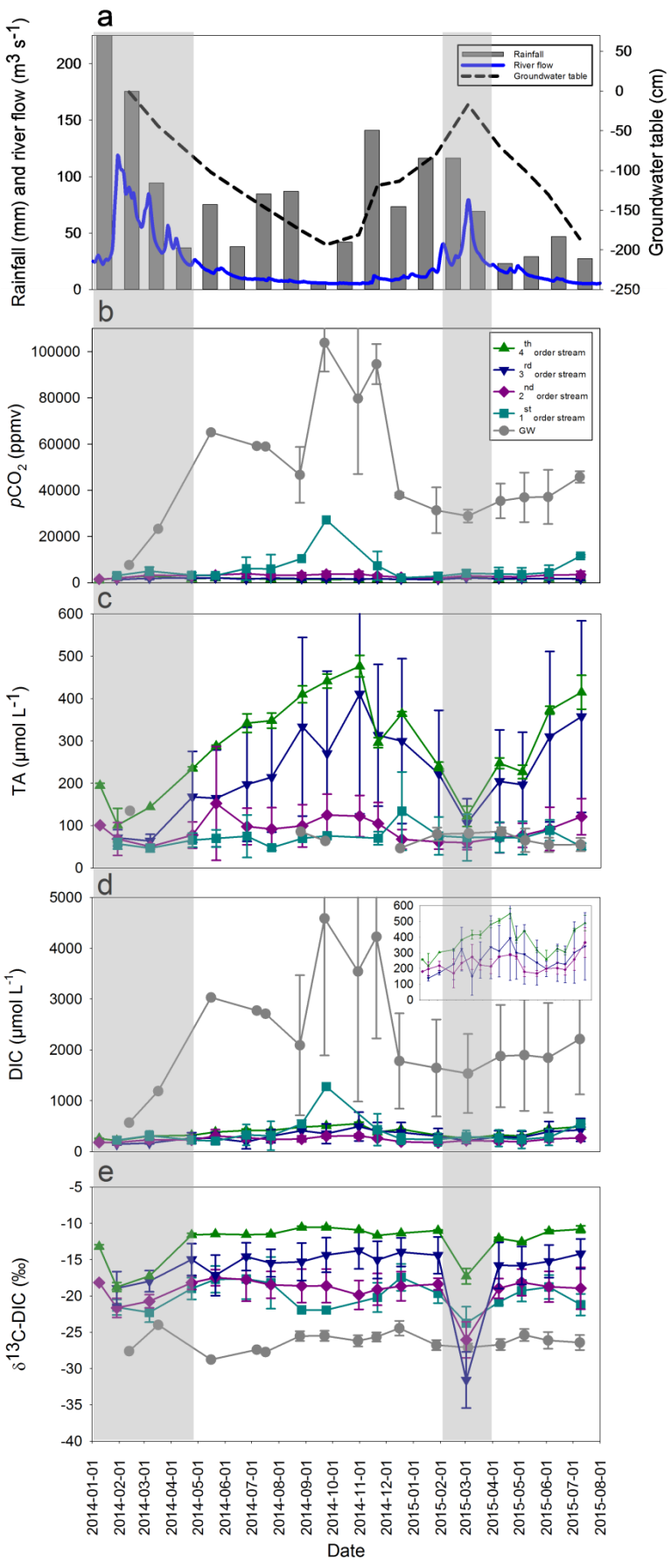

1112

1113 FIGURE 2

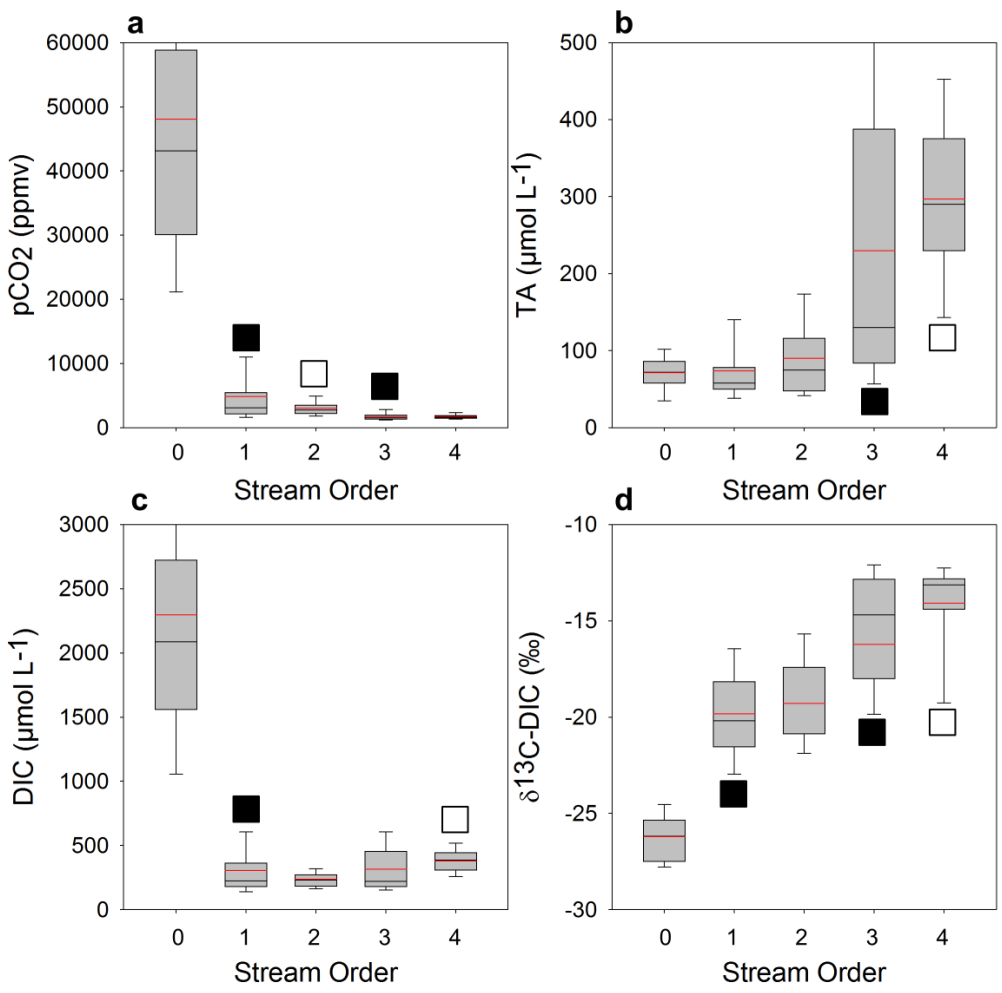

1114

1115

1116 FIGURE 3

1117

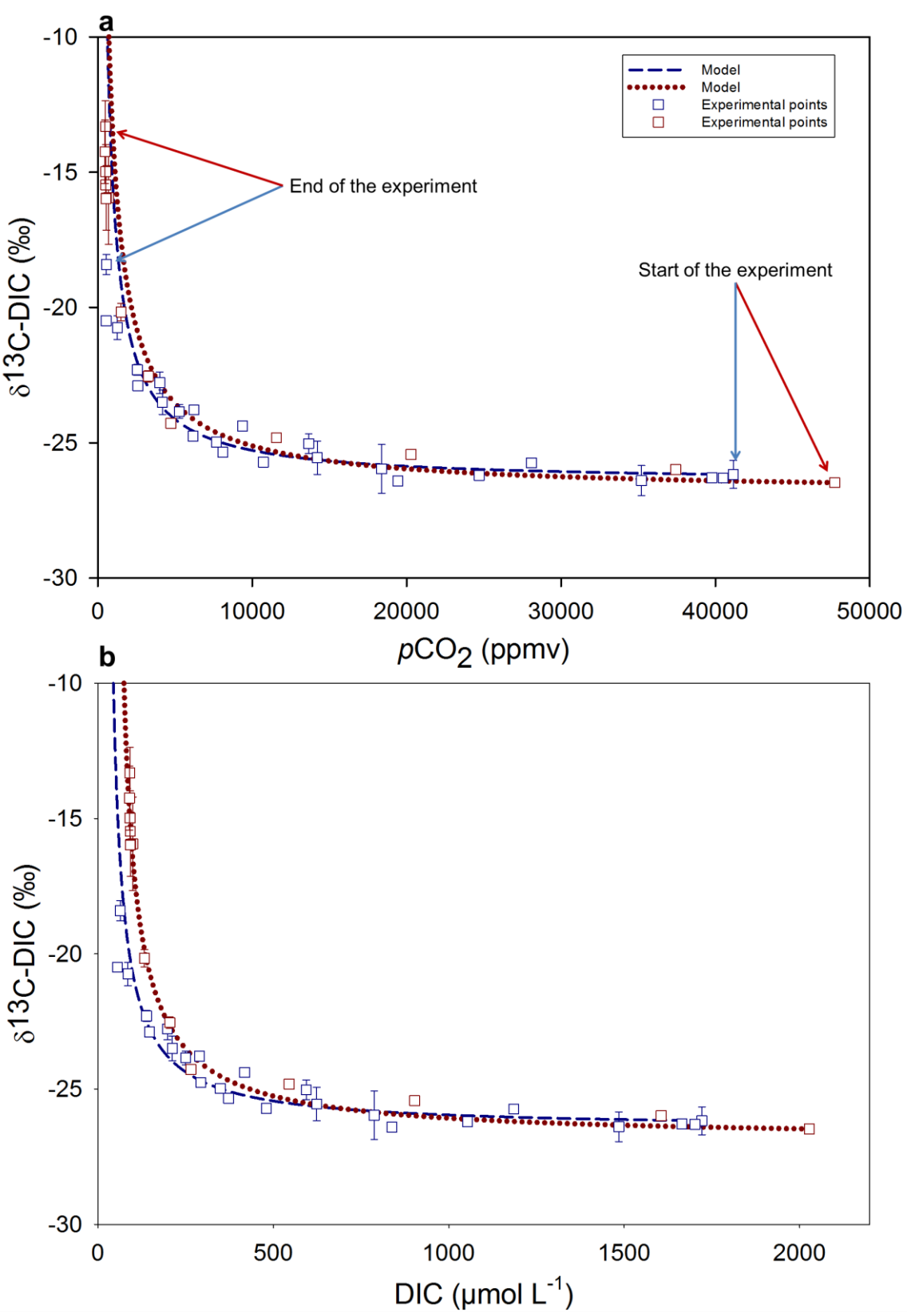

1118

1119

1120 FIGURE 4

1121

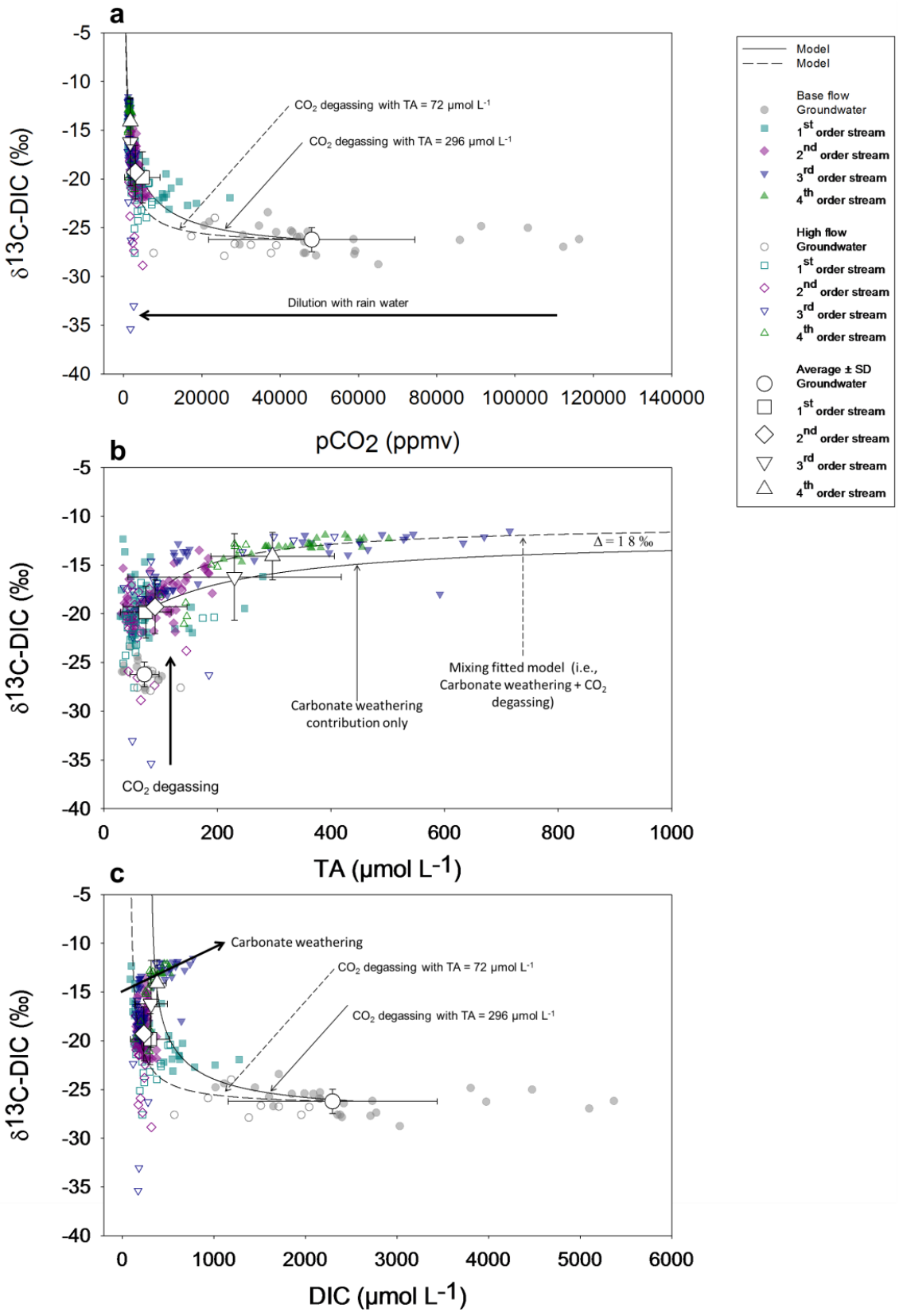

1122

1123

1124 FIGURE 5

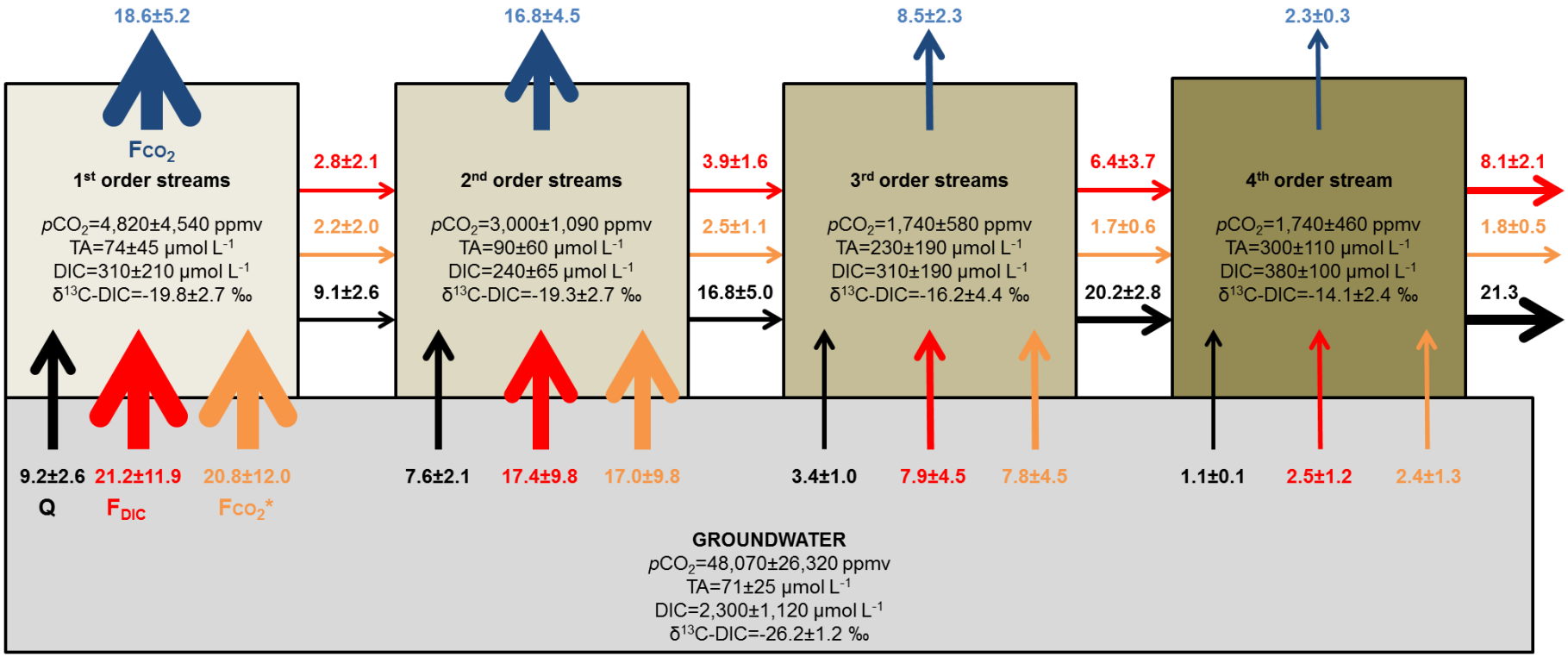

1125

1126

1127

1128 FIGURE 6